

ANALYSIS OF BIMETAL-BASED THERMAL ENERGY HARVESTER USING PIEZOELECTRIC MATERIALS

M.Tech. Thesis

by

SHEKHAR YADAV



**DEPARTMENT OF MECHANICAL ENGINEERING
INDIAN INSTITUTE OF TECHNOLOGY INDORE**

JUNE 2023

ANALYSIS OF BIMETAL-BASED THERMAL ENERGY HARVESTER USING PIEZOELECTRIC MATERIALS

A THESIS

*Submitted in partial fulfillment of the
requirements for the award of the degree
of*
Master of Technology

by

SHEKHAR YADAV



**DEPARTMENT OF MECHANICAL ENGINEERING
INDIAN INSTITUTE OF TECHNOLOGY INDORE
JUNE 2023**




INDIAN INSTITUTE OF TECHNOLOGY INDORE

CANDIDATE'S DECLARATION

I hereby certify that the work which is being presented in the thesis entitled **ANALYSIS OF BIMETAL-BASED THERMAL ENERGY HARVESTER USING PIEZOELECTRIC MATERIALS**


in the partial fulfillment of the requirements for the award of the degree of **MASTER OF TECHNOLOGY** and submitted in the **DEPARTMENT OF MECHANICAL ENGINEERING, Indian Institute of Technology Indore**, is an authentic record of my own work carried out during the time period from May 2022 to June 2023 under the supervision of Dr. Satyanarayan Patel, Assistant professor, Department of Mechanical Engineering and Dr. Dan Sathiaraj, Assistant professor, Department of Mechanical Engineering.


The matter presented in this thesis has not been submitted by me for the award of any other degree of this or any other institute..

 07/06/2023



Signature of the student with date
(SHEKHAR YADAV)

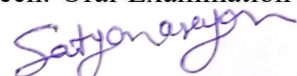
This is to certify that the above statement made by the candidate is correct to the best of my/our knowledge.


 07/06/23
Signature of the Supervisor of
M.Tech. thesis #1 (with date)
(Dr. Satyanarayan Patel)

 08/06/23
Signature of the Supervisor of
M.Tech. thesis #2 (with date)
(Dr. Dan Sathiaraj)

SHEKHAR YADAV has successfully given his/her M.Tech. Oral Examination held on **25 May, 2023**.

 
Signature(s) of Supervisor(s) of M.Tech. thesis
Date: 08/06/23


Signature of Convener, DPGC
Date: 08/06/23


Signature of PSPC Member #1
Date: 08/06/2023


Signature of PSPC Member #2
Date: 08.06.2023

Dedicated to my Parents

Acknowledgments

I would like to express my deepest gratitude and acknowledge research guide **Dr. Satyanarayan Patel**, Energy Materials Lab, and **Dr. Dan Sathiaraj**, for his continuous guidance, patience, motivation, and enthusiasm. **Dr. Satyanarayan Patel** valuable advice, constructive criticism, extensive discussions, and immense knowledge helped me to build a basic understanding of the subject and accomplish my thesis. His research methodology for developing practical applications has been inspiring. During my time of association with him, I learned many things, both in life and career. He has tremendous multi-tasking and man-management skills, which I would like to learn and carry with me in life. He has been a mentor who is always true to his position.

I want to thank **Prof. Suhas Joshi**, Director, IIT Indore, and **Prof. Shanmugam Dhinakaran**, Head of Department, Mechanical Engineering, for supporting the sophisticated facilities to conduct research. I would also like to thank PSPC members **Dr. S Janakiraman** and **Dr. Srimanta Pakhira** for their precious assessment time and valuable comments and suggestions for enhancing research work. I sincerely thank **Dr. Satyanarayan Patel**, DPGC convener, for his support.

Also, I would like to admire my colleagues for their constant care and endorsement throughout this period. My sincere appreciation extends to my lab mates from PhD, Nishchay Saurabh and lab mates for their help and support during my work. I would also acknowledge my friends Soumya Raghuwanshi, Shubham Kumar and Ashwani Kumar for being my constant support during my highs and lows.

Finally, I would like to express my deepest gratitude and respect to my parents for introducing me to this world and my sister Ragini and brother Mukhar for being an ever-supportive rock in my life with their unflinching support.

Abstract

A bimetallic cantilever with a piezoelectric patch at the top surface was used for thermal energy harvesting. The reciprocating nature of the heat source was modeled by providing sinusoidal temperature variation to the stationary heat source. The temperature of the heat source oscillated between 45 °C to 145 °C. Heat transfer from the heat source to the bimetallic beam was modeled using heat transfer in solids and fluids and laminar flow. The finite element analysis of the parameter variation of the bimetallic piezoelectric energy harvester was done in COMSOL. The parameters affecting the geometrical and substrate material properties were analyzed. In this regard, the effect of a difference in the coefficient of thermal expansion (CTE) of the bimetallic beam, length and position of the piezoelectric patch was observed to increase power output. Similarly, parameters such as the difference in density, the bimetallic beam's thermal conductivity, and the piezoelectric patch's thickness decreased the power output. Power law was used to fit the variation of power with different parameters. Finally, two empirical relations were built to analyze the power variation with geometrical and substrate parameters.

TABLE OF CONTENTS

Chapter 1: Introduction

| | | |
|------|--|----|
| 1.1 | Introduction | 1 |
| 1.2 | Characterization of piezoelectric materials | 2 |
| 1.3 | The constitutive laws of piezoelectric materials | 3 |
| 1.4 | Applications of piezoelectric materials | 4 |
| 1.5 | Necessity of energy harvesting | 5 |
| 1.6 | Ways of piezoelectric energy harvesting | 6 |
| 1.7 | Modes of piezoelectric energy harvester | 8 |
| 1.8 | Bimetallic beam | 8 |
| 1.9 | Piezoelectric waste thermal energy harvesting | 9 |
| 1.10 | Literature review | 10 |
| 1.11 | Material for energy harvesting | 12 |
| 1.12 | Research objectives | 12 |

Chapter 2: Modeling Validation and Simulation

| | | |
|-------|--|----|
| 2.1 | Design and operating Principle | 15 |
| 2.1.1 | Mechanism of the heating cycle of heat source | 17 |
| 2.1.2 | Schematic of a bimetallic beam | 18 |
| 2.2 | FEM geometry and simulation in COMSOL | 19 |
| 2.2.1 | Geometry preparation and material assignment in COMSOL | 20 |

| | |
|---|----|
| 2.2.2 Finite element method COMSOL simulation | 22 |
| 2.2.3 Modeling | 24 |
| 2.3 Validation of bimetallic-based piezoelectric energy harvester | 26 |

Chapter 3: Variation of Power with Substrate Material Parameter

| | |
|---|----|
| 3.1 Optimization of resistance | 31 |
| 3.2 Temperature variation | 32 |
| 3.3 Power variation with a coefficient of thermal expansion (CTE) | 34 |
| 3.4 Power variation with thermal conductivity of bimetal | 35 |
| 3.5 Power variation with a density of bimetal | 36 |

Chapter 4: Variation of power with geometric parameter

| | |
|--|----|
| 4.1 Power variation with beam thickness of bimetal | 37 |
| 4.2 Power variation with a thickness of PZT | 39 |
| 4.3 Power variation with length of PZT | 40 |
| 4.4 Power variation with a position of PZT patch | 42 |
| 4.5 Power variation with the width of PZT and beam | 44 |

Chapter 5: Conclusion and future scope

| | |
|------------------|----|
| 5.1 Conclusions | 48 |
| 5.2 Future scope | 49 |
| References | 50 |

List of figures

| Figure no. | Figure Captions | Page no. |
|-------------------|--|-----------------|
| 1.1 | Relation between ferroelectric, pyroelectric and piezoelectric materials | 1 |
| 1.2 | Cantilever beam type PEHs | 6 |
| 1.3 | Circular diaphragm type PEHs | 6 |
| 1.4 | Cymbal type PEHs | 6 |
| 1.5 | Stack-type PEHs | 7 |
| 1.6 (a) | Unimorph type PEHs | 7 |
| 1.6 (b) | Bimorph type PEHs | 7 |
| 1.7 | Modes of piezoelectric energy conversion from input stress based on the relative direction of electric polarization and stress | 8 |
| 1.8 | Bimetallic beam deflection as temperature increases | 9 |
| 2.1 | Schematic side view of bimetallic cantilever beam | 16 |
| 2.2 | 3D schematic of heat cycle in bimetallic cantilever beam energy harvesting | 17 |
| 2.3 | Heating and cooling of bimetallic energy harvester | 18 |
| 2.4 | Schematic and side view of bimetallic beam | 19 |
| 2.5 | FEM model geometry in COMSOL | 20 |
| 2.6 | Source temperature versus time plot | 21 |
| 2.7 | Validation results (a) beam temperatures achieved by the beam, (b) deflection of the beam, (c) voltage achieved by the beam | 27 |
| 2.8 | (a) Model used in validation, (b) Model used in the whole simulation | 28 |
| 3.1 | Power as a function of resistance | 32 |

| | | |
|-----|---|----|
| 3.2 | Plots of source temperature versus time at various temperature differences. | 32 |
| 3.3 | (a) Variation of beam temperature difference versus time and (b) beam temperature difference as a function of source temperature difference | 33 |
| 3.4 | (a) Plots of power versus time at source temperature differences and (b) power as a function of beam temperature differences | 33 |
| 3.5 | (a) Variation of von-Mises stress versus time at CTE difference, (b) Plots of voltage versus time at CTE difference | 34 |
| 3.5 | (c) Plot of power versus time at various CTE differences and (d) power versus coefficient of thermal expansion | 35 |
| 3.6 | (a) power as a function of time at thermal conductivity difference and (b) power versus thermal conductivity | 36 |
| 3.7 | (a) Plots of power versus time at various density differences and (b) power as a function of density difference | 36 |
| 4.1 | Schematic diagram showing bimetallic thickness variation | 38 |
| 4.2 | 2 (a) Beam thickness effect on stress produced on the surface of PZT, (b) Effect of beam thickness on power generated in bimetallic piezoelectric energy harvester | 38 |
| 4.3 | Schematic diagram shows piezoelectric patch thickness increases | 39 |
| 4.4 | (a) Variation of power versus time at a thickness of PZT increases and (b) effect of PZT thickness on power generated in bimetallic piezoelectric energy harvester. | 40 |

| | | |
|------|---|----|
| 4.5 | Schematic diagram shows piezoelectric patch length increases | 41 |
| 4.6 | (a) represents the variation of power with time by changing the length of PZT, and (b) the Effect of PZT length on power generated in bimetallic piezoelectric energy harvester | 41 |
| 4.7 | Schematic diagram shows piezoelectric patch position changing | 42 |
| 4.8 | (a) Power as a function of time at different positions of PZT and (b) effect of PZT position on power generated in bimetallic piezoelectric energy harvester. | 43 |
| 4.9 | Schematic of increase in width of piezoelectric patch and beam | 44 |
| 4.10 | (a) Plots of power as a function of time at various widths of PZT and beam, (b) effect of PZT and beam width on power generated in bimetallic piezoelectric energy harvester | 45 |

List of Table

| Table no. | Table Captions | Page no. |
|------------------|---|-----------------|
| 2.1 | Initial design parameters of piezoelectric energy harvester | 22 |

Chapter 1: Introduction

1.1 Introduction

The dielectric materials are classified into three subcategories: Piezoelectric materials are the subset of dielectric materials and pyroelectric materials are the subset of the piezoelectric materials. Pyroelectric materials act as a bridge between piezoelectric and ferroelectric materials. Figure 1.1 shows the relationship between these materials[1]. All the ferroelectric materials come under pyroelectric materials, showing the pyroelectric effect and all pyroelectric come under piezoelectric materials consisting of piezoelectricity. The crystalline structure of the materials affects their behaviors as piezoelectric, pyro-, and ferroelectric materials. Stress, temperature, or an external electric field can affect the crystal's symmetry, which leads to the induction of spontaneous electric polarization.

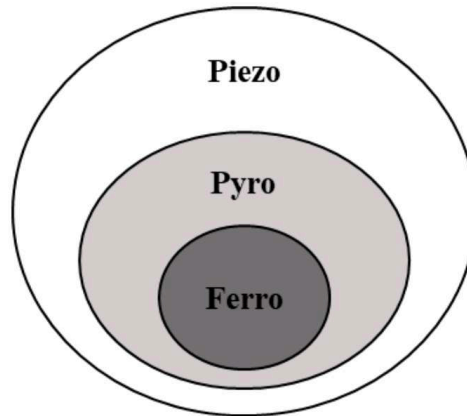


Figure 1.1: Relation between ferroelectric, pyroelectric and piezoelectric materials [17].

A class of materials called piezoelectric materials can produce an electric charge in response to mechanical strain or stress. On the other hand, when an electric field is introduced, they can also experience mechanical deformation[2, 3]. The separation of positive and negative charges within the material's lattice results from the material's asymmetric crystal structure [4].

The asymmetry in their crystal structure (non-centrosymmetric) produces the piezoelectric effect[5]. A centrosymmetric crystal has inversion symmetry because of how the atoms or ions are arranged. This means that if inverted the crystal around its center, the crystal structure would stay unaltered[6]. In contrast, the crystal structure of piezoelectric materials lacks the characteristic of inversion symmetry. Positive and negative charges are distributed asymmetrically inside the crystal lattice due to the lack of inversion symmetry. The occurrence of the piezoelectric effect requires this asymmetry[7, 8]. There are two primary categories of piezoelectric materials: natural and artificial[9]. Quartz, tourmaline, and several ceramics are naturally occurring piezoelectric materials. Artificial materials like polyvinylidene fluoride (PVDF) and Lead zirconate titanate (PZT) are used in a variety of applications[10].

1.2 Characterization of piezoelectric materials

Piezoelectric effect: The piezoelectric effect is found in some materials that generate an electric charge in reaction to mechanical stress or strain and vice versa. Pierre and Jacques Curie made the initial discovery in 1880. The name "piezoelectric" comes from the Greek verb "piezein," which means to push or squeeze[11]. A piezoelectric material's internal crystal lattice structure deforms under mechanical stress or strain, such as bending, stretching, or compression. An electric polarization is produced due to this deformation, which causes positive and negative charges to separate and realign within the material. The opposite direction of the piezoelectric effect is also possible. A piezoelectric substance will deform or change shape when an electric field is applied. It is often referred to as the electrostrictive effect or the inverse piezoelectric effect.

Piezoelectric coefficients: Coefficients that quantify the piezoelectric behavior of materials are known as piezoelectric coefficients. The piezoelectric charge coefficient (d), the piezoelectric strain coefficient (d), and the piezoelectric voltage coefficient (g) are some of these

coefficients. These coefficients determine the strength of the piezoelectric effect in a material [12].

Polarity and crystal orientation: A material's piezoelectric effect is influenced by the structure and orientation of its crystals. The degree of piezoelectric response varies between different crystal orientations[13].

1.3 The constitutive laws of piezoelectric materials

Piezoelectric materials are characterized by three constitutive equations[14].

- I. Direct piezoelectric effect:** This equation connects the mechanical stress or strain applied (T) to the electric charge created in the material (Q). In mathematical terms, it can be written as $Q = d \times T$ or $Q = d \times S$, where d is the piezoelectric charge coefficient. This equation explains how mechanical stress or strain is directly converted into an electric charge.
- II. Inverse piezoelectric effect:** This equation explains how an applied electric field (E) mechanically causes a material to deform or strain (S). $S = d \times E$, where d is the piezoelectric strain coefficient, can be used to represent it. This equation shows how an electric field can be transformed from mechanical deformation in the opposite direction.
- III. Dielectric behavior:** This equation links the permittivity of the material (ϵ) and the applied electric field (E) to the induced polarization (P) in the material. It can write as $P = \epsilon \times E$. This equation explains how the material's polarization responds to an applied electric field.

Combine constitutive laws which describe the combined effect of electrical and elastic mechanical behavior are given below

$$S = sT + d^t E \quad (1.1)$$

$$D = dT + \epsilon E \quad (1.2)$$

where T is stress tensor (N/m^2); S is strain, D is electric displacement (C/m^2), s is elastic compliance matrix evaluated at the constant electric field (m^2/N), d is a matrix of piezoelectric strain coefficients (m/V), ϵ is permittivity (free body dielectric constant) (N/V^2), E is the electric field strength

1.4 Applications of piezoelectric materials

Piezoelectric materials find widespread applications in various fields due to their unique properties. Some notable applications include[15]:

- I. Sensors and actuators:** In sensors and actuators which measure pressure, force, acceleration, and vibration, piezoelectric materials are often utilized. Piezoelectric motors, pressure sensors, and accelerometers are a few examples of the gadgets that use them.
- II. Energy harvesting:** Piezoelectric materials can be used in energy harvesting devices to power small electronic devices or wireless sensors because they can transform mechanical vibrations and environmental vibrations into electrical energy. They are utilized in self-powered sensors, wearable technology, wireless sensor networks and many other applications.
- III. Medical imaging and therapy:** Piezoelectric transducers are essential parts of ultrasonic imaging systems to produce and detect sound waves for creating precise images of inside organs and tissues. Additionally, they are used in targeted ultrasound therapy equipment.
- IV. Sonar and acoustic devices:** Hydrophones, acoustic emission sensors, and underwater sonar systems use piezoelectric materials for detection, measurement, and communication. They make it possible to produce and detect sound waves in aquatic settings.
- V. Piezoelectric igniters:** These substances serve as a dependable and prompt igniting source in piezoelectric igniters for gas stoves, lighters and other gas-powered products.
- VI. Structural health monitoring:** Systems for monitoring the structural health of buildings, bridges, and aircraft use piezoelectric sensors to identify and track structural deformations, vibrations,

and cracks. They aid in preserving the strength and security of buildings.

VII. Piezoelectric microphones: Microphones use piezoelectric materials to convert sound waves into electrical impulses. They are frequently used in many communication and audio recording equipment.

1.5 Necessity of energy harvesting

Piezoelectric energy harvesting is necessary for several reasons, a few are discussed below[16].

- **Utilization of ambient vibrations:** The world around us is full of ambient vibrations, including mechanical vibrations from machinery, automobiles, structures, and even atmospheric vibrations like wind and ocean waves. We can capture and transform this otherwise useless mechanical energy into useful electrical energy via piezoelectric energy harvesting.
- **Sustainable and renewable energy:** A sustainable and renewable energy source is provided by piezoelectric energy harvesting. It lowers dependency on conventional power sources, such as fossil fuels, and assists in reducing carbon emissions and environmental effects by transforming mechanical vibrations into electrical energy.
- **Energy harvesting from human activities:** It is also possible to use piezoelectric energy harvesting to collect energy from human activity. For instance, piezoelectric materials incorporated into footwear or apparel can transform mechanical energy produced during walking or movement into electrical energy, which can power portable gadgets or charge batteries.
- **Maintenance-free operation:** Piezoelectric energy harvesting systems have a long operational lifespan and require little maintenance once installed.
- **Miniaturization and integration:** Piezoelectric materials can be integrated into small and compact devices due to their thin and flexible nature.

1.6 Ways of piezoelectric energy harvesting

There are many ways of harvesting piezoelectric energy in different structural forms [17]. (i) Cantilever beam type, (ii) circular diaphragm type, (iii) cymbal type and (iv) stack type.

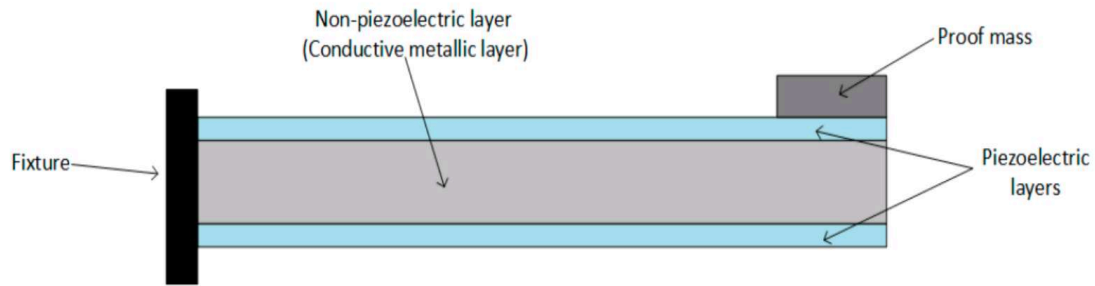


Figure 1.2: Cantilever beam type PEHs[17].

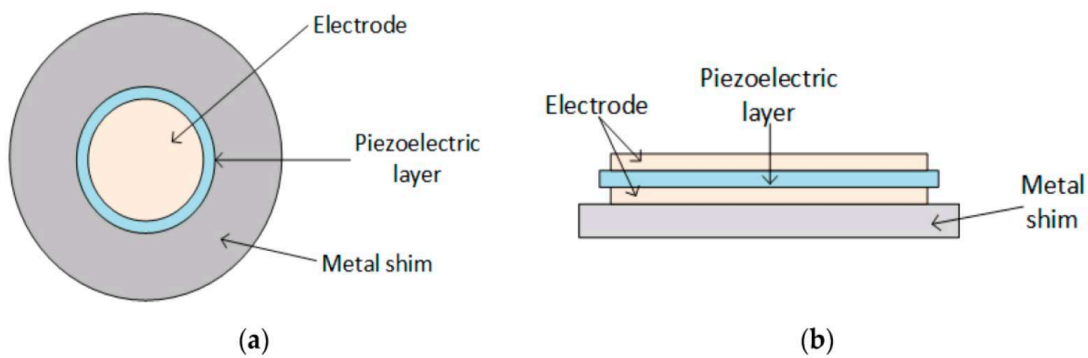


Figure 1.3: Circular diaphragm type PEHs [17].

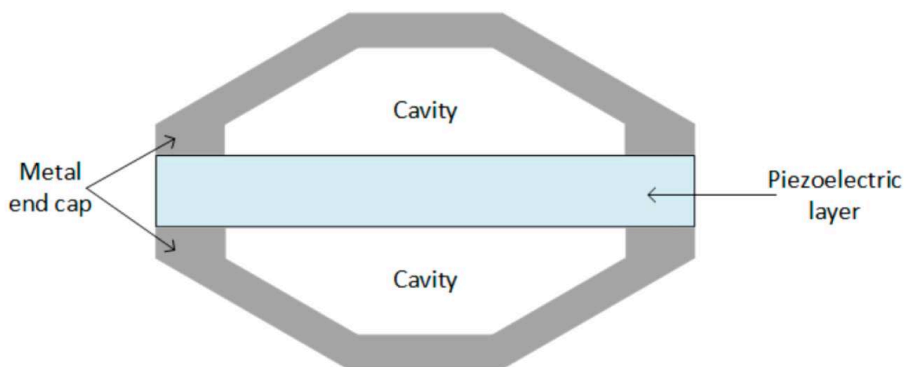


Figure 1.4: Cymbal type PEHs [17].

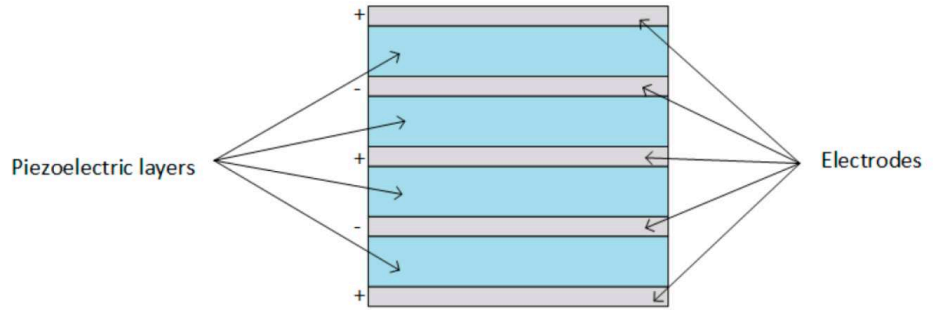


Figure 1.5: Stack-type PEHs [17].

In cantilever beam-type PEHs, different structures are used for energy harvesters, like unimorph, bimorph, and bimetallic-based PEHs.

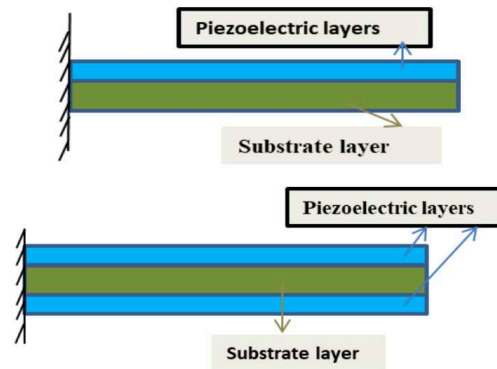


Figure 1.6 (a) Unimorph and (b) Bimorph type PEHs [17].

The piezoelectric layer in a unimorph design shown in Figure 1.6 (a) is usually sandwiched between two electrodes, one linked to the piezoelectric material and the other to the passive substrate. The piezoelectric layer produces an electric charge or voltage due to the piezoelectric effect whenever the device is subjected to mechanical stress or vibration.

- Two piezoelectric layers are joined together with a neutral plane in the bimorph design shown in Figure 1.6 (b). When subjected to vibrations, the bimorph structure bends due to the differential strain between the two layers, producing electric charges. It is possible to obtain energy by bending and deforming the material.
- Bimetallic-based piezoelectric thermal energy harvesting converts thermal energy into electrical energy using

piezoelectric materials and temperature gradient-induced mechanical strain in a bimetallic structure.

1.7 Modes of piezoelectric energy harvester

In piezoelectric energy harvesting, d_{31} and d_{33} modes are frequently employed, distinguished by the piezoelectric coefficient values d_{31} and d_{33} , respectively. These coefficients describe the relationship between mechanical strains or deformation and a piezoelectric material's electrical charge or voltage. The coefficients (d_{31} and d_{33}) represent the induced charge or voltage ratio to the applied strain[18]. In d_{31} mode, the direction of generated polarization is perpendicular to the applied external force. The charge or voltage produced in the perpendicular direction of applied strain is shown in Figure 1.7. While in d_{33} mode, the polarization is generated along the applied external strain and the charge or voltage is also produced in the same direction.

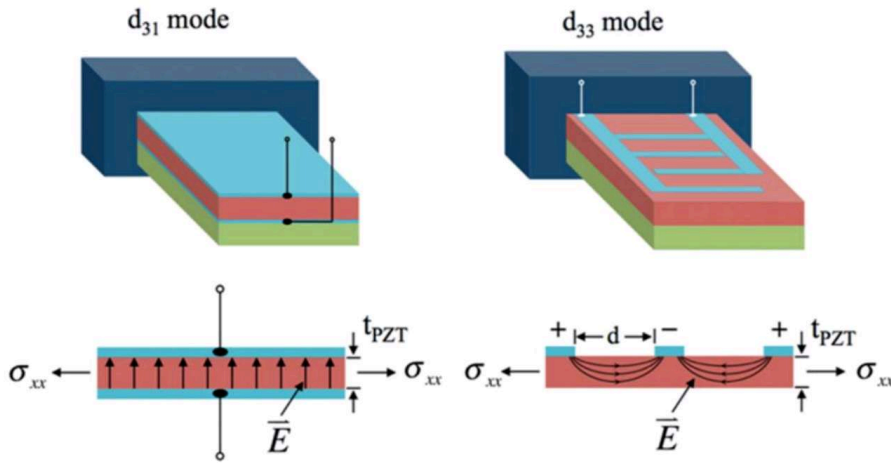


Figure 1.7 Modes of piezoelectric energy conversion from input stress based on the relative direction of electric polarization and stress[19].

1.8 Bimetallic beam

Thermal bimetals are double metal layers, one layer has a high coefficient of thermal expansion (CTE), known as the active layer, and the other has a low one, known as the passive layer, shown in Figure 1.8. When the temperature rises, the active

layer expands more than the passive layer. Thus the active layer generates more thermal strain than the passive one, resulting in the bending of the bimetal. This is also known as the bi-metal effect. The passive layer is loaded in traction, while the active one is loaded in compression since its expansion is restrained.

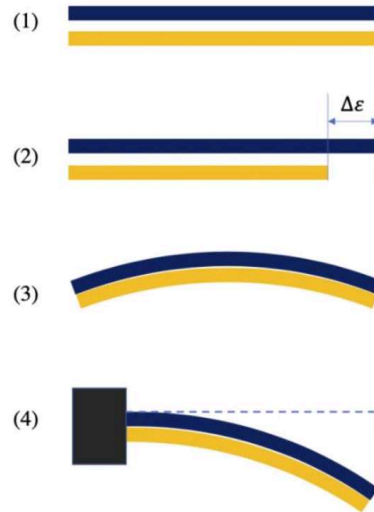


Figure 1.8: Bimetallic beam deflection as temperature increases

1.9 Piezoelectric waste thermal energy harvesting

Thermal energy from waste heat is one of many energy sources with promise due to its abundance and ubiquity. Due to equipment inefficiencies, waste heat is ultimately produced in heat engines and industrial operations [20]. Thermal energy harvesters that use body heat for wearable technology have recently received much attention due to their sustainability[21]. An established commercial technique for harvesting thermal energy is thermoelectric generation. P- and n-type semiconductors comprise the thermoelectric device, which uses the Seebeck effect to transform temperature gradients into electrical current[22]. Thermoelectric materials should have a high Seebeck coefficient, high electrical conductivity, and low thermal conductivity for optimal energy conversion efficiency. However, because these qualities are interrelated, achieving the ideal values for the material is challenging[23].

Due to its excellent efficiency, the pyroelectric effect has been researched as a possible substitute for the thermoelectric effect[24, 25]. There is a review of pyroelectric energy harvesting technologies in[26]. While thermoelectric materials require a difference in temperature over space, pyroelectric materials generate an electric charge when temperature changes occur over time. Finding an environment with temporal temperature change is the key condition for pyroelectric harvesting.

1.10 Literature review

After replacing the pyroelectric material with the piezoelectric material on the bimetallic-based piezoelectric energy harvester

- Hunter et al. introduced MEMS-based pyroelectric energy harvesters with a cantilever structure. A substrate, a pyroelectric material layer, and two proof masses are the main components of the cantilever. Due to the differing thermal expansion coefficients of the pyroelectric material and the metal electrode, the cantilever behaved like a bimetallic strip[27].
- Ravindran et al. presented A tiny pyroelectric generator having a reciprocating motion between a heat source and a heat sink. A bistable membrane and an enclosed chamber with air as the working fluid made up the generator. Air expansion or contraction in the chamber causes the membrane to transition from one condition to another. The generator started to move as a result of this[28].
- Cottrill et al. used the diurnal temperature variation in a desert to directly apply an induced temperature change environment to a thermal energy collecting apparatus. This device did not utilize the pyroelectric effect in any case. For a thermoelectric generator, the variations in the ambient temperature are transformed into a spatial temperature difference. In some experiments, a self-oscillating energy harvester generates

temporal fluctuations using the spatial temperature differential from a fixed heat source[29].

- Chun et al. created a thermo-magneto-electric generator. The phase transition of soft ferromagnetic material between a heat source and a heat sink at about the Curie temperature powered the generator. Although pyroelectric energy harvesting was different from the planned application for this generator, this work also offered a technique for converting a fixed heat source into temperature changes over time. However, a heat sink must provide a significant enough temperature difference to cause motion in these self-oscillating harvesters[30].
- In studies carried out in a vacuum chamber, Hunter et al. simulated the cantilever at 10, 50, and 150 K temperature differences. The difference in temperature between Chun et al.'s was 80 K. and Ravindran et al.'s generators was 79.5 K [27, 28, 30].
- Induced temperature variation used on harvesters was also studied in other reports. Zhang et al. created a thin film pyroelectric device using a laser as a heat source. Wireless power transmission is possible with this technique. The harvester has a low heat flux and low power production when no heat sink[31].
- Polyvinylidene fluoride (PVDF) with shape memory alloys (SMA) was suggested by Gusarov et al.. The PVDF polymer was bonded with a composite on both sides. As SMA went through its phase transition in response to the temperature change, stress was produced by the resulting deformation. As a result, the output voltage increased by 77% when piezoelectricity was present[32].
- Lee et al. [33] and You et al. [34] provided experimental findings on electrical energy produced using both mechanical stress and thermal energy simultaneously. However, there needs to be more research concentrating on design or mechanism.

- In order to combine thermoelectric and pyroelectric effects, Kim et al. [35] presented a wearable hybrid generator. Various hybrid generators have been reported; however, most of the time, each effect was only tested in static or individually regulated settings.

1.11 Material for energy harvesting

Piezoelectric material is used for energy harvesting, allowing them to convert mechanical input into electrical output energy efficiently. A few examples of commonly used piezoelectric energy harvester materials are discussed here[1].

- 1) Lead Zirconate Titanate (PZT): PZT has high piezoelectric coefficients, which means it can produce a large amount of electrical output energy in response to mechanical input energy.
- 2) Polyvinylidene Fluoride (PVDF): PVDF is a famous organic piezoelectric material for energy harvesting. It has comparatively low-value piezoelectric coefficients than PZT, but it has the advantage of more flexibility.
- 3) Aluminum Nitride (AlN): AlN is a ceramic piezoelectric substance becoming more popular for energy-harvesting uses. It has good mechanical qualities, a high piezoelectric coefficient, and superb thermal conductivity.
- 4) Zinc Oxide (ZnO): Another piezoelectric substance utilized in energy harvesting is ZnO. It has good piezoelectric qualities and a wide bandgap. ZnO is a cost-effective solution for some energy-collecting applications due to its low cost.

1.12 Research objectives

We are using FEM simulation to see the power variation in a bimetallic-based piezoelectric energy harvester with the properties of a bimetal, geometric parameter of the bimetallic beam and piezoelectric material patch. After finding all the variations, an empirical relation has to be developed in two parts.

(i) Substrate material parameter variation:

$$P = C_1 (\Delta\alpha)^{b_1} (\Delta k)^{b_2} (\Delta\rho)^{b_3} (\Delta T)^{b_4}$$

(ii) Geometric parameter variation

$$P = C_2 (x_p)^{v_1} (l_p)^{v_2} (t_b)^{v_3} (t_p)^{v_4} (w_p)^{v_5}$$

where $\Delta\alpha$ is the difference in thermal expansion coefficient, Δk is thermal conductivity, $\Delta\rho$ is the density of bimetal, ΔT is the temperature difference of bimetal, x_p is the position of PZT, w_p is the width of bimetal and PZT, t_b is the thickness of the bimetallic beam, l_p is the length of PZT, t_p is the thickness of PZT, and $b_1, b_2, b_3, b_4, v_1, v_2, v_3, v_4, v_5$ are powers of empirical relation.

Chapter 2: Modeling Validation and Simulation

The bimetallic beam model, its design procedure, and the material used for designing the same for piezoelectric energy harvesting are discussed in the present analysis. After designing the model, the FEM simulation procedure is explained. After the validation of the bimetallic beam model with the previous work, further modification in the model is done and the different variations are performed on the modified model.

2.1. Design and operating principle

The model comprises a simple structure consisting of a bimetallic cantilever beam with a solid piezoelectric material layer attached to the central portion. Figure 2.1 illustrates the basic structure of the piezoelectric energy harvesting model, including the direction of polarization in the bimetallic cantilever. Two different alloys, characterized by significant differences in the coefficient of thermal expansion (CTE), are utilized to construct the bimetallic beam. The piezoelectric material employed in this model is lead zirconate titanate (PZT-5H). This material is specifically chosen for its capability to harvest piezoelectric kinetic energy, such as vibrational or rotational energy. Vibration is typically imparted to the energy harvester through either base excitation or by harnessing the naturally occurring vibrational energy in different working conditions. Various energy sources are available in the environment, with waste heat thermal energy being utilized to induce vibrations in our model. Waste thermal energy, which is abundantly present in the environment, arises predominantly from heat engines employed in energy conversion processes, including heat pumps, automobiles, power plants, and locomotives [3]. Machines and several energy-intensive processes produce enormous heat energy as a byproduct [3]. Waste heat can be

divided into high-, medium-, and low-quality recovery chances depending on the temperature range.

Thermal energy harvesters can make use of natural or waste heat. Compared to conventional heat engines, the thermal energy harvester has the advantage of reduced operating and maintenance expenses.

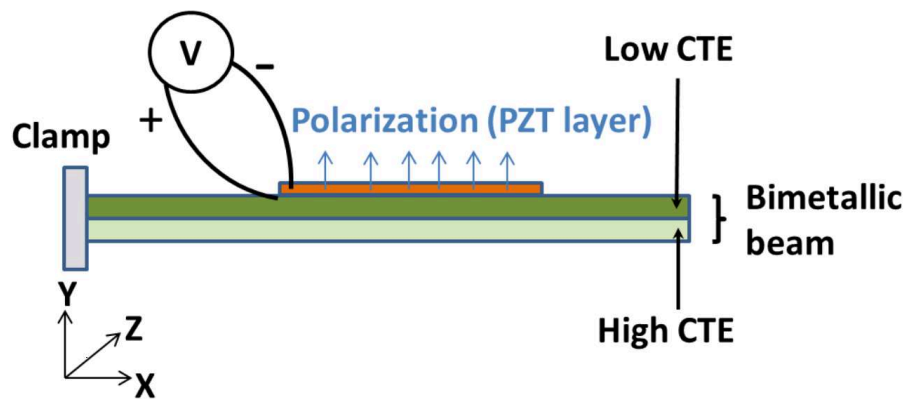


Figure 2.1: Schematic side view of the bimetallic cantilever beam[36].

The bimetallic beam used in the thermal energy harvester, shown in Figure 2.1, has two different alloys with large coefficients of thermal expansion (CTE). When the temperature of the bimetallic beam is increased, the layer of an alloy with a higher CTE value tends to elongate, while the layer with a lower value of CTE does not tend to elongate as much. Since the higher CTE layer is in compression while the lower CTE layer is in tension, the bimetallic beam bends. When the temperature is decreased and the bimetal is allowed to cool, it regains its initial state. However, for the thermal energy harvester using the piezoelectric material, the fluctuation in stress is required for energy harvesting. Since the piezoelectric material is attached to the central portion of the bimetallic beam, the piezoelectric material's stress depends on the bimetallic beam's stress. The stresses in the bimetallic beam mainly depend on the temperature, but for the fluctuation in the

stress of the bimetallic beam, a temporal temperature difference environment is needed.

2.1.1 Mechanism of the heating cycle of heat source

A stationary heat source or a constant temperature with varying positions is required for such a temperature difference.

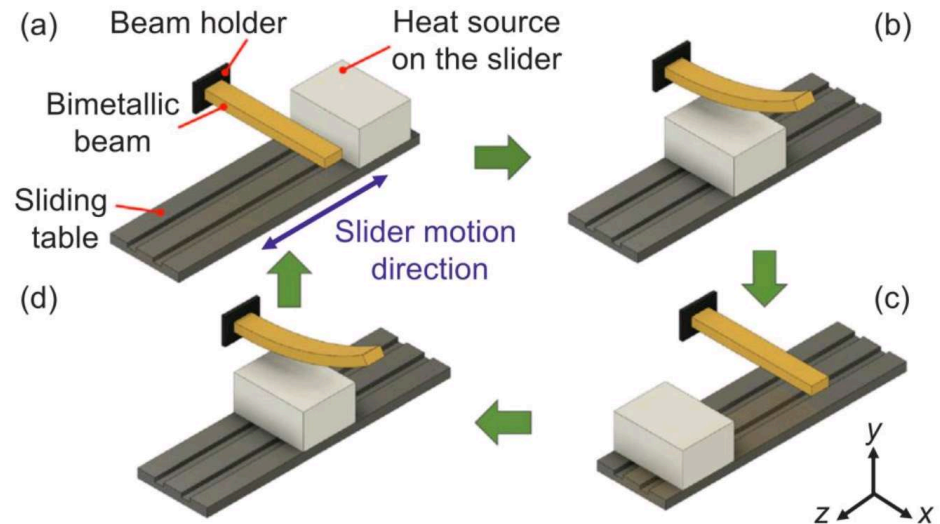


Figure 2.2: 3D schematic of heat cycle in bimetallic cantilever beam energy harvesting[36].

The mechanism of constant temperature with position variation is studied theoretically to understand the bimetallic thermal energy harvester. This mechanism makes temperature fluctuation possible by putting a fixed heat source on a position-controlled slider that oscillates laterally beneath the beam. In order to create temperature variations, the following two scenarios are taken into account. An oscillating structure can be employed in a system with a stationary heat source. Additionally, a heat source that changes in temperature over time, such as a chip (integrated circuit) on a circuit board, may be employed.

Figure 2.2 shows the heat cycle process; figure 2.2 (a) shows the heat source and beam are in the initial position, the beam is in a normal straight position and the heat source is at the end of the slider. Figure 2.2 (b) shows that the heat source is under the beam while passing

beneath the beam. As the heat source starts traveling toward the beam, the transfer of heat takes place, resulting in the temperature of the beam rising slowly and simultaneously, and the bending of the beam takes place, resulting in bending stress. Figure 2.2 (c) shows the heat position at the next extreme side of the slider, which is opposite of the initial symmetric position after passing beneath the beam and it starts traveling back towards the beam. The time in which the heat source returns the beneath beam, the beam releases its stress and again becomes straight and unstressed. Figure 2.2 (d) shows that as the heat source returns towards the beam, heat transfer starts again, generating stress and bending the beam and reaching its initial position. A similar mechanism is followed in each heating cycle. Briefly, figure 2.3 shows heating and cooling.

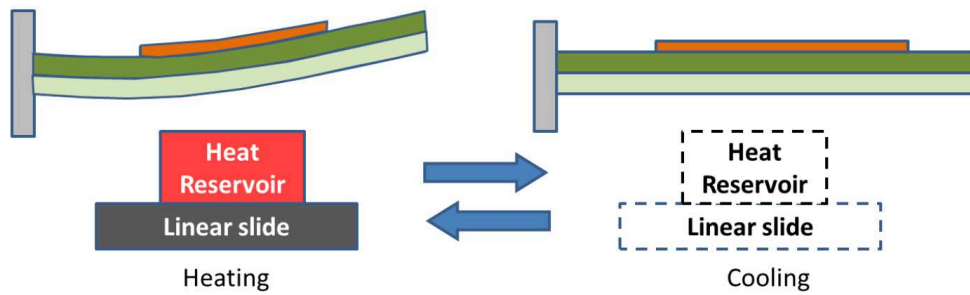


Figure 2.3: Heating and Cooling of the bimetallic energy harvester.

Since the work which is discussed in this project is a FEM simulation-based model, so in the simulation-based it is not possible to follow the basic mechanism of a heating cycle discussed above. So, a proper heating arrangement is provided in the FEM model that will work as a functional operating condition. The FEM model and its initial parameter is discussed below.

2.1.2 Schematic of a bimetallic beam

Figure 2.3 shows the dimensioning of the bimetallic piezoelectric energy harvester and the piezoelectric patch's position for the bimetallic beam. It also shows the piezoelectric energy harvester's complete side view in which the red color block below the bimetallic

beam represents the heat source placed over the slider. The heat source is placed transverse to the beam so that heat can be transferred very easily to the beam and the layer with the high CTE tends to extend more than the layer with low CTE. The layer having the high CTE is known as the active layer and the layer with the low CTE is known as the passive layer. When the heat transfer takes place from the heat source to the beam, the temperature of the beam starts rising and the active layers experience more thermal strain than the passive one, as a result of which bending of the beam takes place properly and generates stresses can make piezoelectric material to produce maximum voltage. The empty portion shown below in Figure 2.3, the gap between the bimetallic beam and the heat source, is filled by the air to fulfill the essential medium requirement for heat transfer. The heat can easily be transferred from the heat source to the bimetallic beam through conduction and convection.

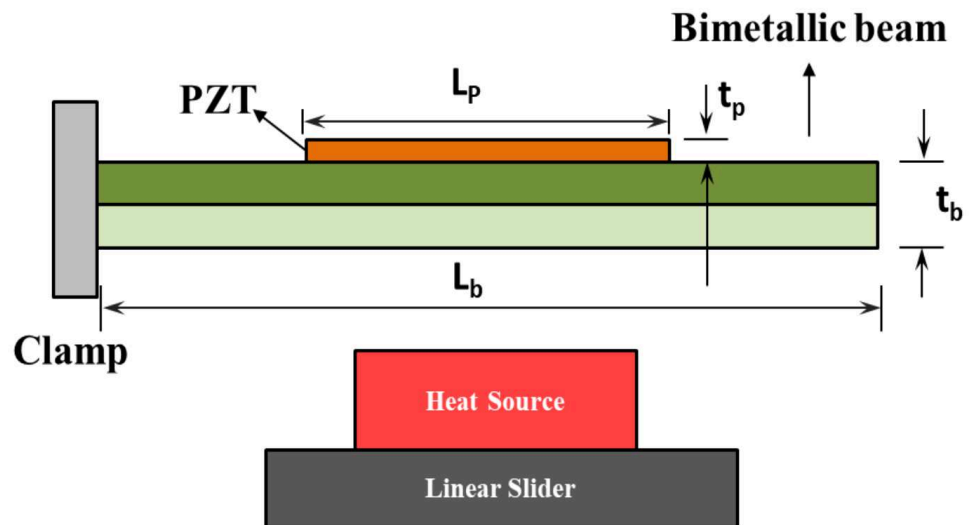


Figure 2.4: Schematic and side view of the bimetallic beam

2.2 FEM geometry and simulation in COMSOL

The geometry is prepared in the COMSOL software and then the simulation is performed by applying the different boundary conditions. Moreover, the thermal energy harvester model is validated with the existing model.

2.2.1 Geometry preparation and material assignment in COMSOL

The complete model geometry is made using the block form method in the COMSOL simulation software. The bimetallic beam is formed first, having the dimension of 50 mm in length, 14 mm in wide and 0.15 mm depth of each layer of the bimetallic beam. The two layers of the bimetallic beam are made up of such metallic alloy having a considerable difference in the coefficient of thermal expansion (CTE). The 5 mm length of the bimetallic beam is in the clamped conditions, which is treated as the cantilever beam. In COMSOL, it is clamped by using the fixed boundary condition from each surface of the initial 5 mm length of the bimetallic beam. Clamps are kept at a room temperature of 298.15 K.

The piezoelectric material (PZT-5H), having the dimension of 26 mm in length, 14 mm wide and 0.127 mm deep, is placed over the central portion of the bimetallic beam. The piezoelectric material is divided into small patches of 2 mm in length for validating the model with the existing model. The initial design parameters used to make the piezoelectric energy harvester are given in Table 2.1.

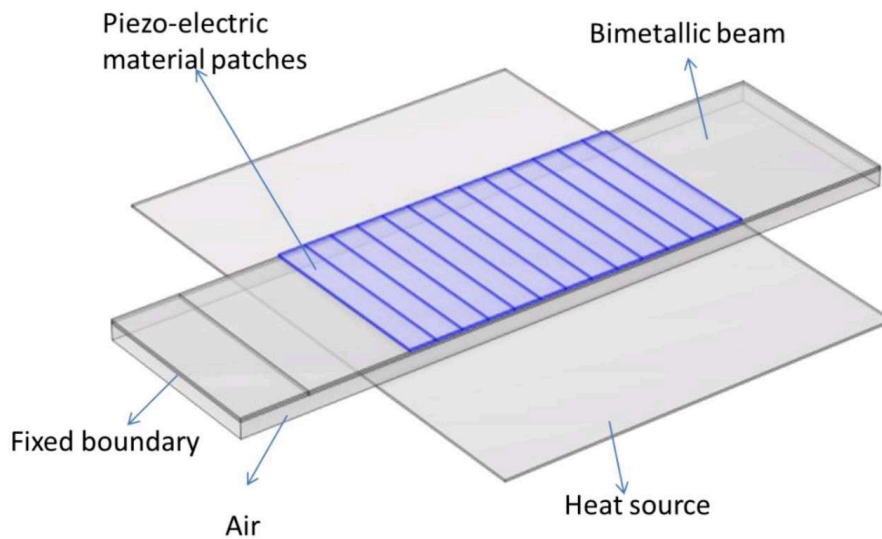


Figure 2.5: FEM model geometry in COMSOL

The stationary heat source is made up of copper, which has a dimension of 40 mm in length, 30 mm wide and 0.15 mm deep, placed transverse to the bimetallic beam. The surface is uniformly heated or cooled, which is how the heat source was simulated. The heat is given by the heat source having the time-dependent temperature form with 95°C mean temperature and which having the fluctuation of 50°C given in the form of the sinusoidal form having the frequency of 0.02 Hz is the minor frequency used in the simulation of piezoelectric energy harvester which is used for the validation of our energy harvester. The temperature is given in sinusoidal form in the below equation and Figure 2.6 shows the variation of source temperature concerning the time.

$$T = 368 + 50\sin((2 \times \pi \times 0.02 \times t) - 89.2) \quad (2.1)$$

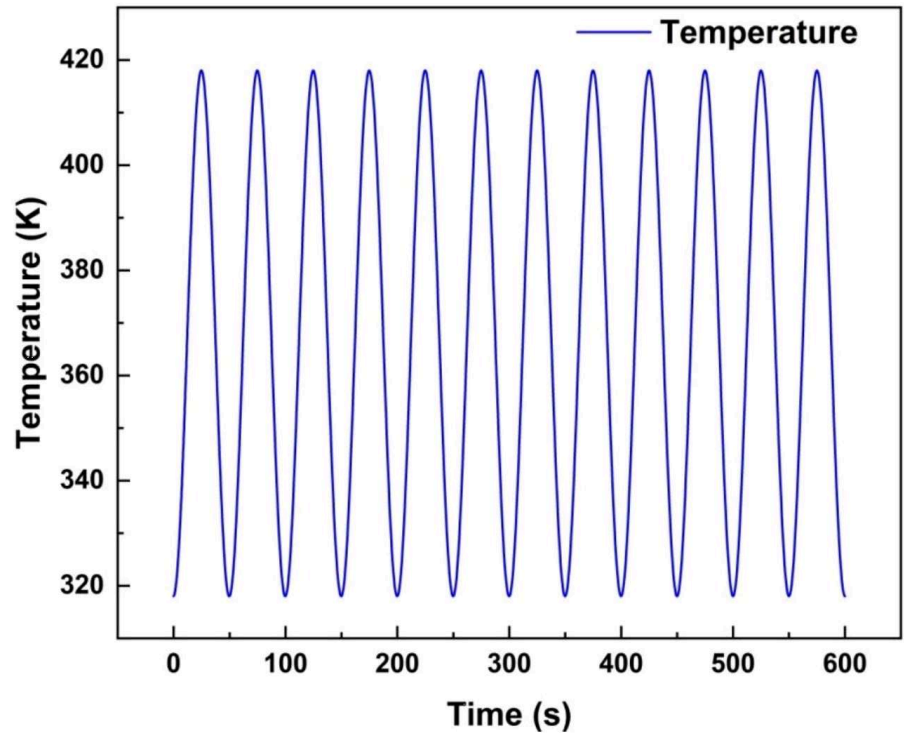


Figure 2.6: Source temperature versus time plot.

The cuboidal block having the dimension (50×14×1 mm³) is shown in Fig 2.5 placed between the bimetallic beam and the heat source is

filled with the air for the transfer from the heat source to the bimetallic beam.

Table 2.1: Initial design parameters of piezoelectric energy harvester[36].

| Symbol | Description | Value |
|------------------|---|---|
| $L_b \times b_b$ | Bimetallic beam size | $50 \times 14 \text{ mm}^2$ |
| $L_p \times b_p$ | PZT layer size | $26 \times 14 \text{ mm}^2$ |
| L_c | Length of clamp | 5 mm |
| t_b | The thickness of the bimetallic beam | 0.3 mm |
| t_p | The thickness of the PZT layer | 0.127 mm |
| t_a | The thickness of the air gap | 1 mm |
| f | Specific deflection | $0.6 \times 10^{-6} \text{ K}^{-1}$ |
| E_b | Young's modulus of bimetal | 172 GPa |
| E_p | Young's modulus of PZT | 50 GPa |
| E_e | Effective Young's modulus of the beam | 172 GPa |
| d_{31} | Piezoelectric strain coefficient of PZT | $-320 \times 10^{-12} \text{ m/V}$ |
| p | Pyroelectric coefficient | $-400 \mu\text{C}/(\text{m}^2\text{K})$ |
| | Dimension of heat source | $30 \times 40 \times 0.15 \text{ mm}^3$ |

2.2.2 Finite element method COMSOL simulation

COMSOL Multiphysics 6.1 has been used for FEM simulation in order to analyze the mechanism. The entire mechanism uses heat transfer dynamics, which is critical to analyze. For simplicity, a frequency of 0.02 Hz is used for the entire simulation to get an enormous temperature difference and deflection of the beam. The time-dependent temperature given to the heat source remains constant throughout the entire simulation for validation and further variation simulations. This COMSOL multiphysics model combines two multiphysics to analyze the heat transfer mechanism, a module of Heat transfer in Solids and Fluids (*ht*) and Laminar flow (*spf*). This combination of modules is used to analyze the heat transfer between the heat source and the bimetallic beam through the air boundary block. The open boundary

condition flows the heat in and out through the air block after transferring heat to the bimetallic beam.

As the temperature of the bimetallic beam is increased, the nature of the bimetallic beam is to get deflected and generate stress on the cantilever beam and the piezoelectric patch. The piezoelectric layer. Analysis of the charge produced in the entire mechanism combination of Solid mechanics (*solid*) and Electrostatics (*es*) modules is used. In Solid Mechanics module boundary conditions, in Fixed Constraint initial 5 mm of the beam is clamped and 45 mm remains free in the form of the cantilever beam. In the piezoelectric material section, the constitutive relation is used in the Strain-charge form for ready availability of piezoelectric material properties (PZT – 5H). In the Electrostatics module boundary conditions, charge conservation on the piezoelectric material is applied. The top surface of piezoelectric material is defined as the terminal and the bottom surface is defined as ground. The terminal chosen is of circuit type and the resistance of 50 MΩ is placed between the terminal and the ground.

Since heat transfer and distribution are critical in temperature distribution in COMSOL multiphysics simulation. For transferring the heat in solids heat transfer module is used. The time-dependent energy equation is given as follows:

$$d_z \rho C_p \frac{\partial T}{\partial t} + d_z \rho C_p u \cdot \nabla T + \nabla T \cdot q = d_z Q + q_0 + d_z Q_{ted} \quad (2.2)$$

where ρ is the density (kg/m^3), T is the absolute temperature (K), Q is the power density, C_p is heat capacity ($J/(kgK)$), u is the velocity (m/s), Q_{ted} is the thermoelastic damping, q_0 is the inward heat flux and q represents the heat flux vector

$$q = -d_z k \nabla T \quad (2.3)$$

where k is the thermal conductivity ($W/(m.K)$). This is Fourier's law of heat conduction. The laminar flow module is based on Navier-Stokes equations as follows:

$$\frac{\partial \rho}{\partial t} + \nabla(\rho u_2) = 0 \quad (2.4)$$

$$\rho \frac{\partial u_2}{\partial t} + \rho(u_2 \nabla)u_2 = \nabla \left[-\rho I + \mu(\nabla u_2 + (\nabla u_2)^T) - \frac{2}{3}\mu(\nabla u_2)I \right] + F + \rho g \quad (2.5)$$

where u_2 is the velocity (m/s), p is the pressure (Pa), F is the volume force vector (N/m^3), g is the acceleration of gravity, μ is the dynamic viscosity (Pa.s), I is the unity tensor. Equation (2.4) is the continuity equation and represents the conservation of mass and equation (2.5) represents the conservation of momentum.

2.2.3 Modeling

The behavior of the bimetallic beam is studied under a time-dependent temperature environment. As the beam's temperature increases, the deflection in the beam is produced, which becomes the cause of the development of stress in the bimetallic beam, resulting in voltage generation over the piezoelectric surface. So let us observe how the bimetallic beam behaves under an actual variable temperature environment. In actual practice, the beam has three layers: PZT, bimetal, and adhesive material layer, which combines the PZT layer over the bimetallic beam. The bimetallic beam has two different layers, but E_b in Table 2.1 represents the total Young's modulus of the bimetallic beam. In the multilayered structure, the effective Young's modulus (E_e) is calculated as

$$E_e I = \sum_{i=1}^n E_i I_i \quad (2.6)$$

where the I is the area moment of inertia and the total number of layers is given by n . From the area-moment theorem, the deflection of the cantilever bimetallic beam is given by[36],

$$\delta = \frac{P_{\text{free}} L_b^3}{3E_e I} \quad (2.7)$$

where P_{free} is the point load at the free end of the cantilever beam, $E_e \cdot I$ is the beam flexural rigidity, and $I = b_b t_b^3/12$ is the moment area of inertia. From the equation (2.7), the mechanical load can be calculated as:

$$P_{\text{free}} = \frac{E_e t_b^3 b_b \delta}{4L_b^3} \quad (2.8)$$

where L_b is the length, b_b is the width, and t_b is the thickness of the bimetallic beam. As the temperature of the bimetallic is increased, the beam deflects and the curvature of the beam is given by

$$\frac{1}{R} = \frac{2\delta}{L_b^2 + \delta^2 - t_b \delta} \quad (2.9)$$

where R is the radius of the heated bimetallic beam. Deflection of cantilever clamped beam

$$\delta = \frac{f \Delta T L_b^2}{t_b} \quad (2.10)$$

When the temperature of the beam changes beam deflects and electric charge Q is developed in a piezoelectric layer given by,

$$Q = \frac{F d_{31} L_p}{t_p} \quad (2.11)$$

Strain in the piezoelectric layer is given by $\epsilon_p = \frac{t_b}{2R} = \frac{3}{4} \times \Delta \alpha \times \Delta T$.

Now the force F on the piezoelectric layer is substituting Eq. (2.11),

$$F = \epsilon_p E_p b_p t_b \quad (2.12)$$

Charge Q becomes,

$$Q = \frac{3}{4} \Delta \alpha \Delta T E_p d_{31} L_p \quad (2.13)$$

The model estimates the output voltage across the load resistance,

$$V = \frac{\sum Q}{C_p} \quad (2.14)$$

where C_p is the capacitance of the piezoelectric layer. Where the difference of CTE of the bimetallic beam is $\Delta\alpha = \frac{4}{3}f$. The maximum power obtained is [20]

$$P = \frac{\left(\frac{V_{oc}}{\sqrt{2}}\right)^2}{R} = \frac{fA_p t_p d_{31}^2}{\epsilon_0 \epsilon_{33}} \quad (2.15)$$

where A_p is the surface area of PZT, R is load resistance across the terminal and ground, ϵ_{33} is the relative permittivity, and V_{oc} is the open circuit voltage across the resistance[36].

2.3 Validation of bimetallic-based piezoelectric energy harvester

The bimetallic piezoelectric energy harvester is modeled, and the material is assigned to all the specific parts of the geometry. Now validating the model, we are providing sufficient boundary conditions and the initial geometric parameters shown in Table 2.1 is used in the model. For validation, COMSOL simulation software is used. The model is designed on the same dimension as used the in the model of Miwon Kang and Eric M. Yeatman [36].

The time variation sinusoidal temperature environment is provided to the heat source, shown in equation (2.1). Temperature variation is studied for the 600 s along the length of the beam until the steady state of oscillation is achieved. For getting the required specific deflection of $f = 0.6 \times 10^{-6} K^{-1}$, the thermal expansion coefficient of the upper layer is kept at $22 \times 10^{-6} K^{-1}$ and the lower metallic layer is kept at $22.8 \times 10^{-6} K^{-1}$. The heat was transferred from the heat source to the bimetallic beam through the air between the bimetallic beam and the heat source. The combination of heat transfer and the laminar flow is used for the air medium of heat transfer. The solid mechanics, electrostatics and electric circuit combine to convert the mechanical vibration or stress into an electric charge. After assigning the boundary condition, four different multiphysics coupling is produced in the COMSOL. Non-isothermal Flow coupling combines the effects of the Laminar Flow and Heat Transfer in solids and fluids, Thermal

Expansion coupling combines the effects of the Heat Transfer in solids and fluids and Solid Mechanics; Piezoelectric effect coupling combines the effect of the solid mechanics and electrostatics and the last that is pyroelectricity multiphysics coupling combines the effect of the electrostatics and heat transfer in solids and fluids.

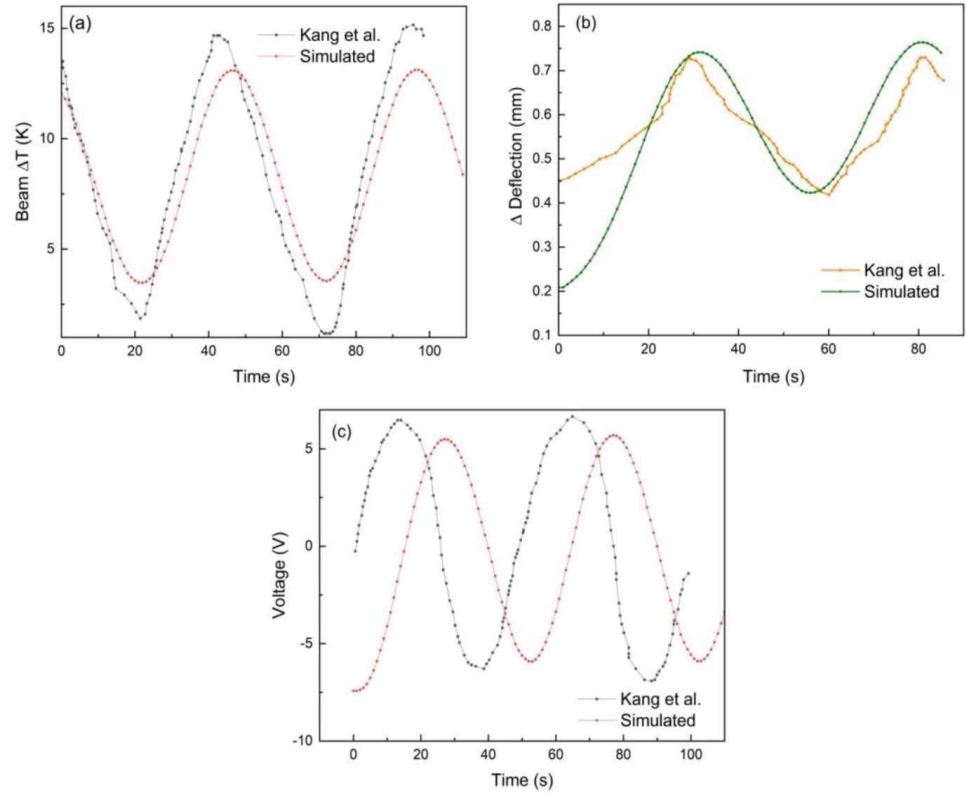


Figure 2.7: Validations results (a) beam temperatures achieved by the beam, (b) deflection of the beam, (c) voltage achieved by the beam.

To simulate with a user-controlled free tetrahedral mesh of different sizes (coarse, coarser, and highly coarse), along with a time-dependent analysis for 600 seconds, and obtain data for temperature achieved by the beam, the deflection produced in the beam and the voltage developed on the surface of the piezoelectric energy harvester. Typically, coarser meshes have fewer elements, reducing simulation times and potentially reducing accuracy. The results obtained are shown in Figure 2.7.

- Under similar experimental conditions, the simulation results obtained are discussed below.

- a) The temperature change of the bimetallic beam achieved using simulation was obtained as $\Delta T = 10.5$ K and the experimental $\Delta T = 12.5$ K.
- b) The deflection of the bimetallic beam obtained using simulation and experiment was 0.32 mm.
- c) The piezoelectric voltage obtained using simulation is 5.7 V and the experimental result is 6.7 V.

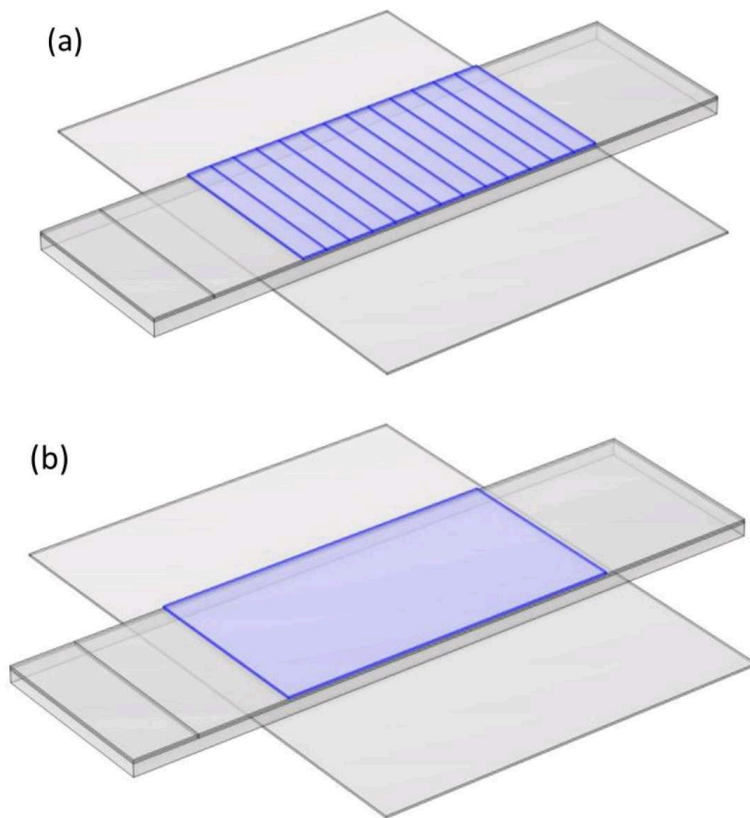


Figure 2.8 (a) model used in validation, (b) model used in the whole simulation.

After the successful validation of our model shown in Figure 2.8 (a) with 13 small patches of PZT, we replace the small patches with bigger ones (b) of the same surface area and volume. It is observed that all validation results, temperature difference of beam, deflection, voltage and the power obtained in both models (a) and (b) are identical. Further, all the variation to achieve objectives is done on model (b) for

obtaining all the objectives. To achieve the all objectives, the required modification in the model was done in every variation. Variation of power with substrate material properties and geometric parameters like length, width, thickness, etc., of beam and PZT has been studied.

Chapter 3: Variation of Power with Substrate Material Parameter

The model is validated successfully and ready to perform further simulation for obtaining the power variation for a geometric parameter and material properties of a bimetallic-based piezoelectric energy harvester. From now onwards, modification has been done at different places to fulfill the research objectives. Now moving towards achieving the first objective of our research, in which variation of power is studied for the properties of bimetallic substrate used in the piezoelectric energy harvester.

3.1 Optimization of resistance

The heat source temperature is kept fixed, as given by equation (2.1) in the previous chapter; all the boundary conditions, physics interface and multiphysics couplings are precisely the same as those used in the simulation to validate the piezoelectric energy harvester. All the simulation is performed on the same model with a single piezoelectric patch structure having the same surface area and volume. Only the resistance is now changed to optimize its value for obtaining more power. The value of resistance is now varying from 20 M Ω to 220 M Ω , keeping the significant difference in the value of the coefficient of thermal expansion (CTE) of the bimetallic beam in the energy harvester, i.e. $\Delta\alpha = 20$ (the upper and lower layer of the bimetallic beam is kept at $2.8 \times 10^{-6} \text{ K}^{-1}$ and $22.8 \times 10^{-6} \text{ K}^{-1}$).

The power variation to the resistance is observed in the bimetallic-based piezoelectric energy harvester in simulation, shown in Figure 3.1. As the value of resistance increases, the power initially increases after achieving the peak power at 100 M Ω , then power decreases. It is because the impedance of external electricity should be matched with the impedance of the piezoelectric material for getting the maximum power output from the bimetallic-based piezoelectric energy harvester.

The impedance is matched at the resistance of 100 MΩ. Now we fixed the resistance at 100 MΩ for all other further variations.

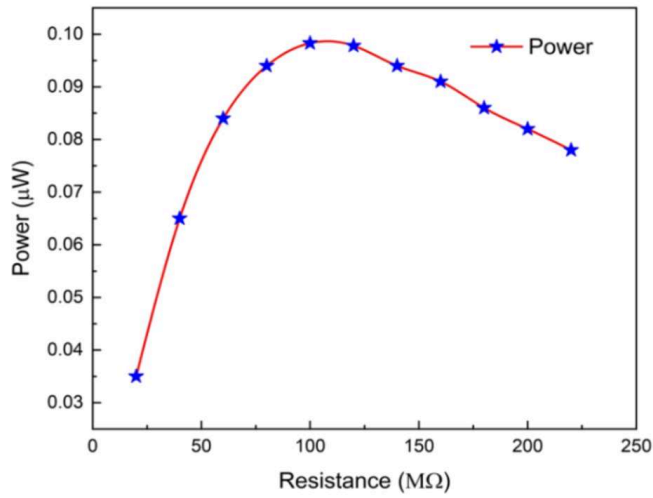


Figure 3.1: Power as a function of resistance.

3.2 Temperature variation

This section observes the variation of power to the temperature achieved by the beam. The variation in the temperature of the beam is necessary to see the variation in the heat source input temperature. The temperature is given to the heat source in the sinusoidal form, given by the equation below.

$$T = 368 + \Delta T \cdot \sin((2 \times \pi \times 0.02 \times t) - 89.2)K \quad (3.1)$$

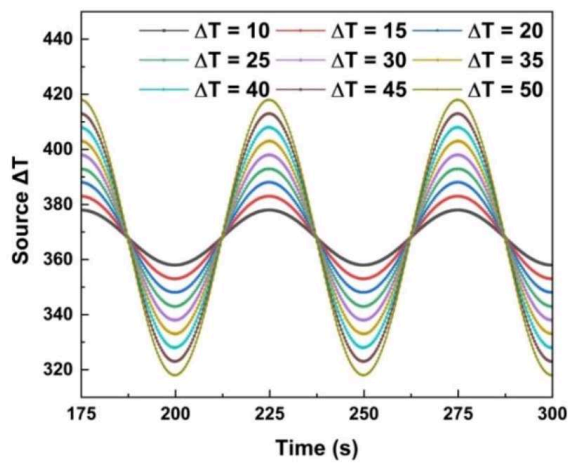


Figure 3.2: Plots of source temperature versus time at various temperature differences.

The amplitude of the temperature of the heat source ΔT is increasing from 10 K to 50 K with an increment of 5 K and the temperature achieved by the beam is observed in the simulation.

The source temperature varies for the time shown in Figure 3.2 and the temperature difference achieved by the beam to the time shown in Figure 3.3(a). The beam temperature achieved concerning the increment in the source temperature is shown in Figure 3.3(b).

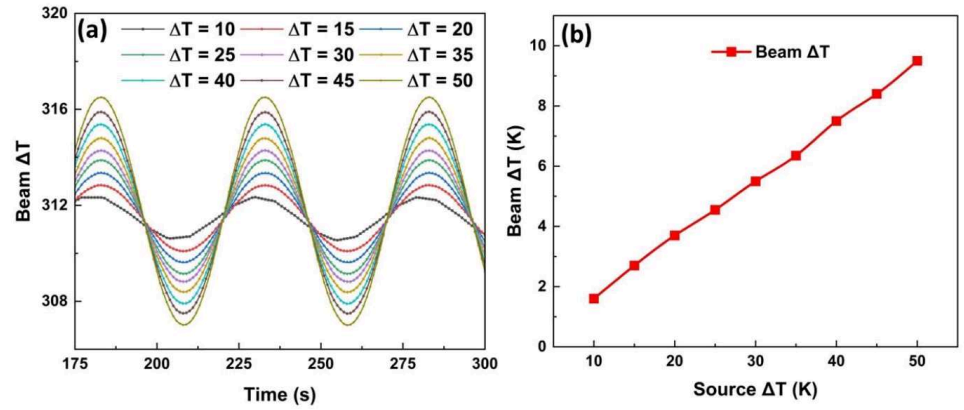


Figure 3.3 (a) Variation of beam temperature difference versus time and (b) beam temperature difference as a function of source temperature difference.

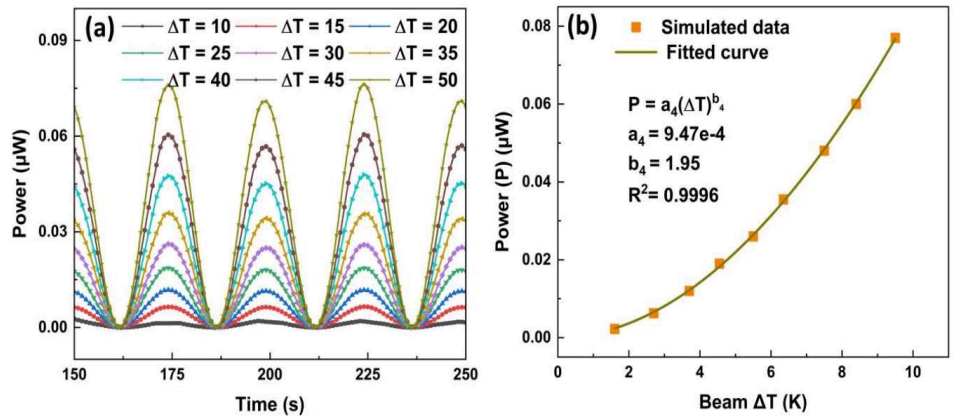


Figure 3.4 (a) Plots of power versus time at source temperature differences and (b) power as a function of beam temperature differences.

The power variation for time and temperature achieved by the beam is shown in Figures 3.4(a) and 3.4(b), respectively. It is observed that as

the temperature of the source increases, the temperature of the beam also increases linearly. Power is also increasing to the temperature achieved by the beam. As the temperature of the bimetallic beam increases, the deflection of the beam also increases because the difference in the CTE is vast, as a result of which stress increases, which increases the voltage and power [36]. Figure 3.4(b) shows that the power law is used for fitting the data obtained of power variation concerning beam temperature difference achieved. Moreover, the relation is obtained for the same. The temperature amplitude of the heat source is fixed at $\Delta T = 50$ K for all other further simulations.

3.3 Power variation with a coefficient of thermal expansion (CTE)

The temperature of the heat source is fixed at the temperature given in equation 3.1, having the amplitude of sinusoidal form equal to $\Delta T = 50$ K. The variation of power for the difference in the CTE of the bimetallic beam is observed. By keeping the CTE of the upper metallic layer is kept constant at $\alpha_u = 2.8 \times 10^{-6} \text{ K}^{-1}$ and changing the CTE of the lower metallic layer from $\alpha_l = 8.8 \times 10^{-6} \text{ K}^{-1}$ to $\alpha_l = 22.8 \times 10^{-6} \text{ K}^{-1}$. It means the difference of CTE ($\Delta\alpha$) increases from the $\Delta\alpha = 6 \times 10^{-6} \text{ K}^{-1}$ to $\Delta\alpha = 20 \times 10^{-6} \text{ K}^{-1}$. The variation of von Mises stress produced in the bimetallic beam, voltage and power generated over the surface of PZT concerning time is observed and shown in Figure 3.5 (a), (b) and (c), respectively.

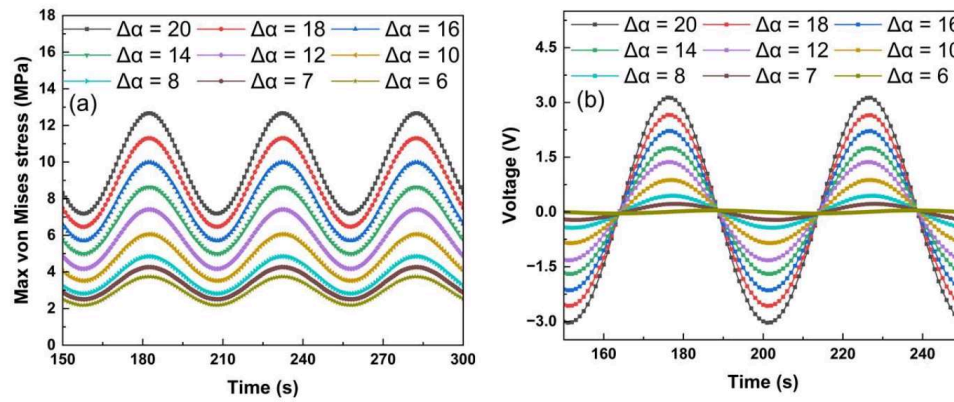


Figure 3.5 (a) Variation of von-Mises stress versus time at CTE difference, (b) Plots of voltage versus time at CTE difference

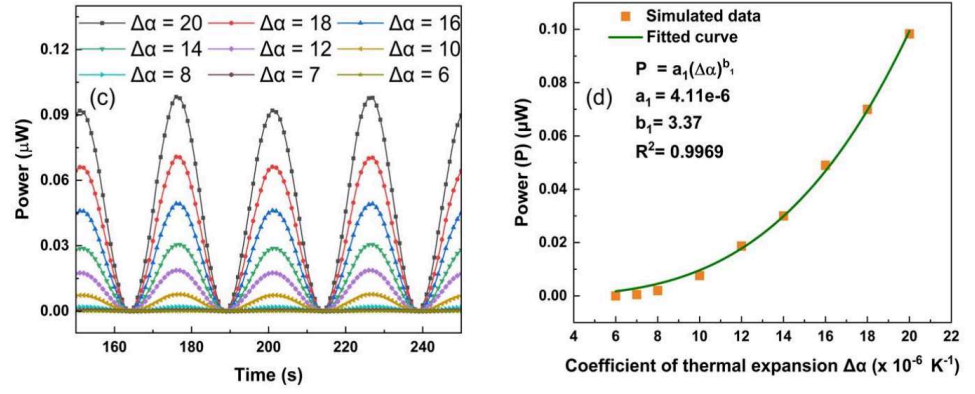


Figure 3.5(c) Plots of power versus time at various CTE differences and (d) power versus coefficient of thermal expansion

As the difference in the CTE of the bimetallic layer increases, the deflection also increases, as a result of which stress increases. Hence, voltage is directly proportional to stress, so voltage and power both increase simultaneously. Figure 3.5 (d) represents the variation of the power to change in CTE and a fitted curve is also provided that provides the relation between power and change in CTE.

3.4 Power variation with thermal conductivity of bimetal

The variation of the bimetal CTE is done and the maximum power is achieved at a large difference in CTE $\Delta\alpha = 20 \times 10^{-6} \text{ K}^{-1}$. It is fixed for all further variations (the CTE of the upper metallic layer is kept constant at $\alpha_u = 2.8 \times 10^{-6} \text{ K}^{-1}$ and the CTE of the lower metallic layer is $\alpha_l = 22.8 \times 10^{-6} \text{ K}^{-1}$). Now the variation in thermal conductivity of the bimetallic layer is observed.

The thermal conductivity of the upper metallic layer is fixed at 10 W/m K and the lower layer's conductivity varies from 50 W/m K to 410 W/m K with an increment of 40 W/m K. As the thermal conductivity of the lower metallic layer increases, the difference between the thermal conductivity of upper and lower layer also increases. After running the simulation, we observed the variation of power to time, and the relation obtained by fitting the curve in data obtained in the simulation is shown in Figures 3.6 (a) and 3.6 (b).

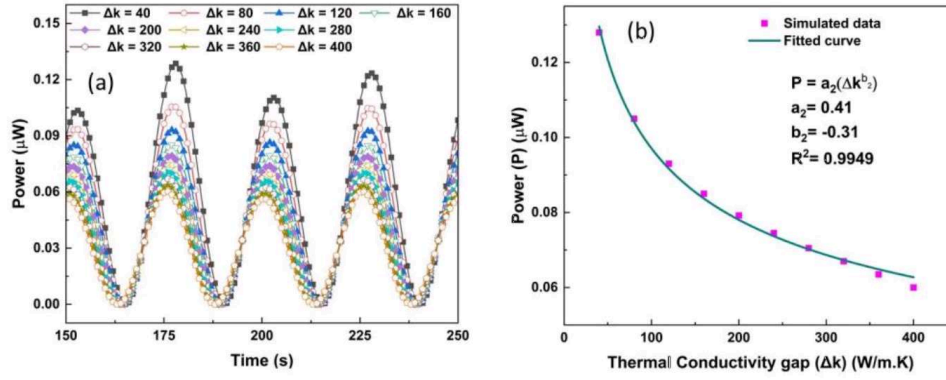


Figure 3.6 (a) power as a function of time at thermal conductivity difference and (b) power versus thermal conductivity

3.5 Power variation with a density of bimetal

The thermal conductivity difference of the bimetallic layer is now kept constant at $\Delta k = 40 \text{ W/m.K}$ ($k_{\text{upper}} = 10 \text{ W/m.K}$ and $k_{\text{lower}} = 50 \text{ W/m.K}$). Now the power variation to density is observed in the simulation. The density of the upper metallic layer is kept constant at 1000 kg/m^3 and the lower metallic layer density varies from 2000 kg/m^3 to 11000 kg/m^3 . It means the differences in lower and upper metallic layer density are slowly increasing. In the simulation, the power variation versus time and density differences is achieved and shown in Figures 3.7 (a) and 3.7 (b), respectively.

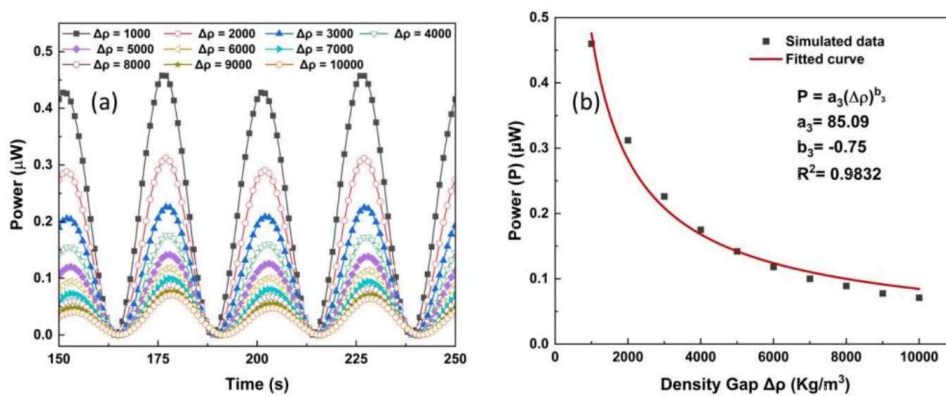


Figure 3.7 (a) Plots of power versus time at various density differences and (b) power as a function of density difference

Chapter 4: Variation of power with geometric parameter

The variation of power with the bimetallic substrate parameter with each property of the bimetallic beam in the piezoelectric energy harvester is varied and observed the effect of each parameter on the power developed in the previous chapter 3. Now after fixing the substrate materials properties like the difference in the coefficient of thermal expansion (CTE) is fixed at $\Delta\alpha = 20 \times 10^{-6} \text{ K}^{-1}$ in which the CTE of the upper metallic layer is fixed at $\alpha_u = 2.8 \times 10^{-6} \text{ K}^{-1}$ and that of the lower metallic layer is kept at $\alpha_l = 22.8 \times 10^{-6} \text{ K}^{-1}$. The thermal conductivity difference of bimetal is fixed at the $\Delta k = 220 \text{ W/m.K}$, in which the thermal conductivity of the upper and lower metallic layer is kept fixed at $k_u = 20 \text{ W/m.K}$ and $k_l = 240 \text{ W/m.K}$ respectively. The density difference of bimetal is fixed at $\Delta\rho = 3000 \text{ kg/m}^3$, in which the density of the upper and lower layer is $\rho_u = 1000 \text{ kg/m}^3$ and $\rho_l = 4000 \text{ kg/m}^3$. The amplitude of the source temperature is also fixed at $\Delta T = 50 \text{ K}$. These properties are fixed for further variation via simulation. Now the power variation with a geometric parameter of the bimetallic energy harvester, like the thickness of the bimetallic beam, thickness, length, width and position of the piezoelectric patch. The FEM simulation study is done to see the power variation to different parameters. Let us see the variation of each parameter one by one.

4.1 Power variation with beam thickness of bimetal

The thickness of each bimetal layer varies by an equal amount from 0.1 mm to 0.75 mm in the model Figure 2.8(b) shown in Chapter 2, keeping the other parameter constant as before. The schematic of thickness variation is shown in Figure 4.1. From Figure 4.2(a) and Figure 4.2(b), it is observed that as the thickness of the beam increases, the maximum stress generated on the surface of PZT and power generated by the bimetallic-based piezoelectric energy harvester decreases. It is due to the reason that as the thickness of the beam increases, the rate of heat transfer decreases. Hence the temperature difference between the bimetallic beams results in reduced deflection.

Power generated by the bimetallic piezoelectric energy harvester is directly proportional to the induced stress, which decreases with reduced deflection. Hence, power is also decreasing.

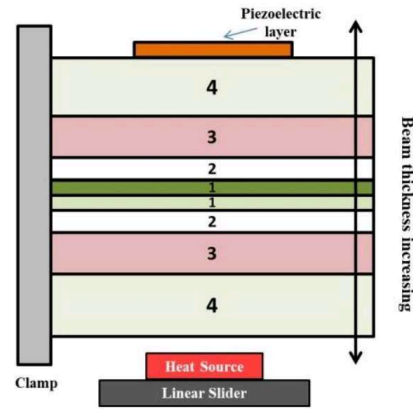


Figure 4.1: Schematic diagram showing bimetallic thickness variation

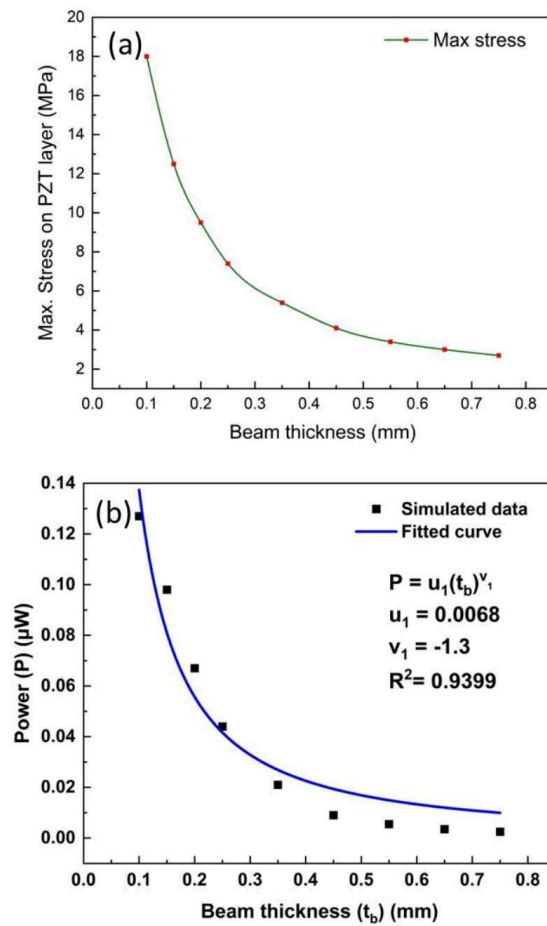


Figure 4.2 (a) Beam thickness effect on stress produced on the surface of PZT, (b) Effect of beam thickness on power generated in bimetallic piezoelectric energy harvester.

Figure 4.2(b) also shows the curve which fits all data points and provides a relation showing the variation of power with changing the thickness of the beam in the bimetallic energy harvester.

4.2 Power variation with a thickness of PZT

The variation of power with the thickness of the bimetallic beam is observed. Now fix the thickness of each bimetallic layer at $t_b = 0.2$ mm for all further variations. The thickness of piezoelectric material in the bimetallic energy harvester increases from 0.1 mm to 1 mm and the piezoelectric patch is placed over the central portion of the bimetal. Figure 4.3 represents the schematic diagram showing how the PZT patch's thickness increases. Figure 4.4 (a) represents the variation of power with time by changing the thickness of PZT. Figure 4.4(b) represents the data obtained from the simulation. The curve fits all the data and provides a relation that directly shows the power variation with increasing the thickness of PZT.

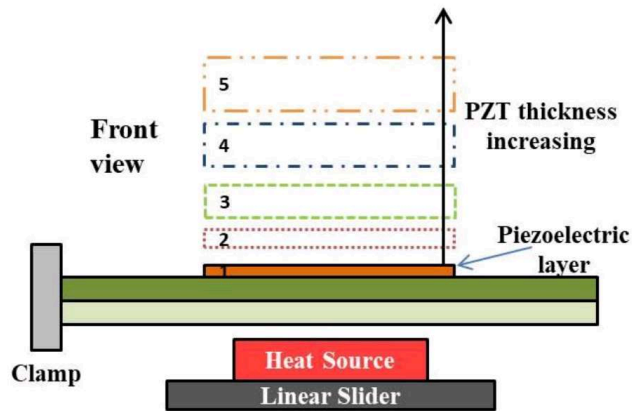


Figure 4.3: Schematic diagram shows piezoelectric patch thickness increases

It is observed that as the thickness of PZT increases, the power decreases. Since equation 2.15 shows the power is directly proportional to the thickness of PZT, power should be increased with thickness increases. However, as the thickness of PZT increases, it resists the bimetal oscillation frequency, which results in reduced

deflection. Hence deflection indirectly reduces the stress generated on the surface of PZT, directly reducing the energy harvester's power.

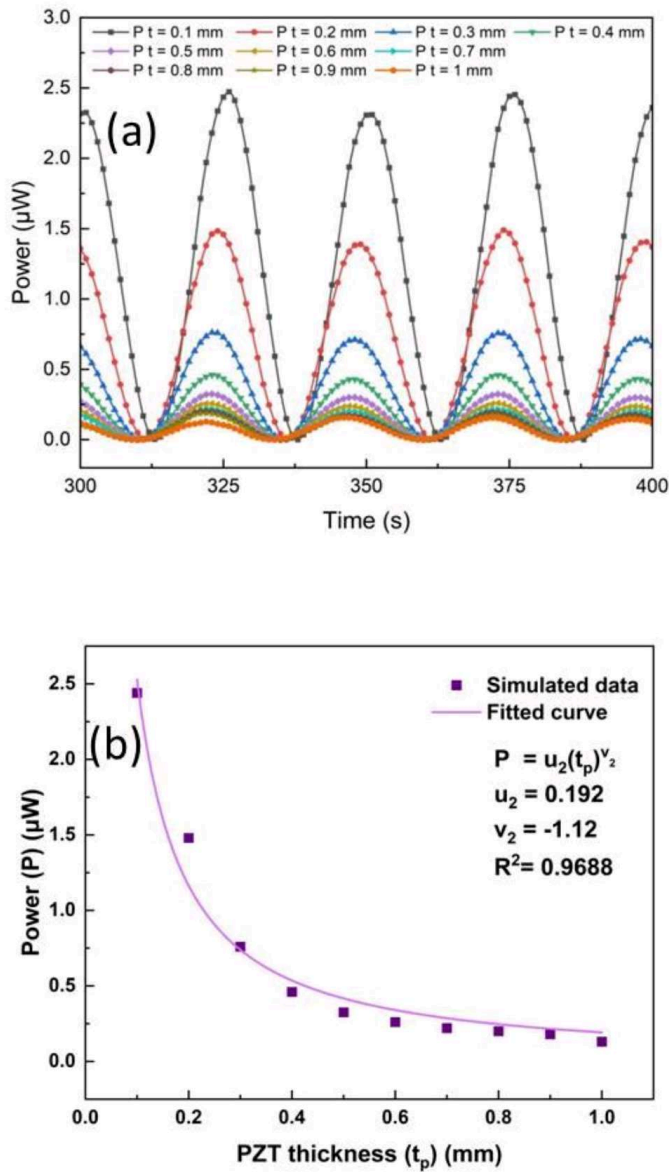


Figure 4.4 (a): Variation of power versus time at a thickness of PZT increases and (b) effect of PZT thickness on power generated in bimetallic piezoelectric energy harvester.

4.3 Power variation with a length of PZT

The thickness of PZT is fixed at 0.15 mm for all further variations. The effect of the length of PZT on the power generated by the bimetallic energy harvester is observed. The length of PZT is changed from 5 mm to 45 mm with an increment of 4 mm. The PZT patch is placed over

the central portion of the bimetal at every length. Figure 4.5 shows the schematics of length variation in the piezoelectric energy harvester.

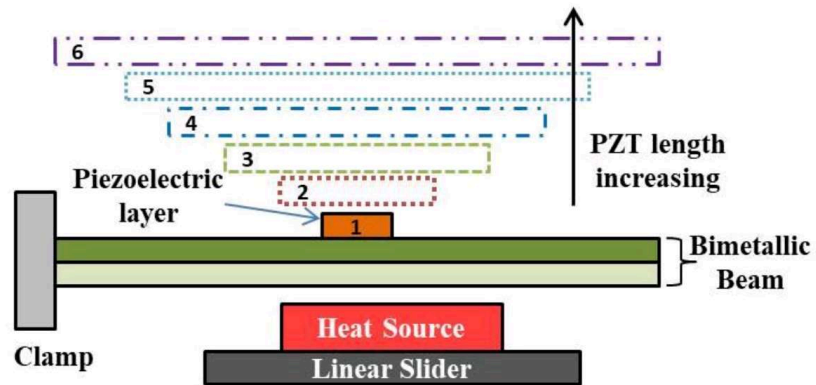


Figure 4.5: Schematic diagram shows piezoelectric patch length increases.

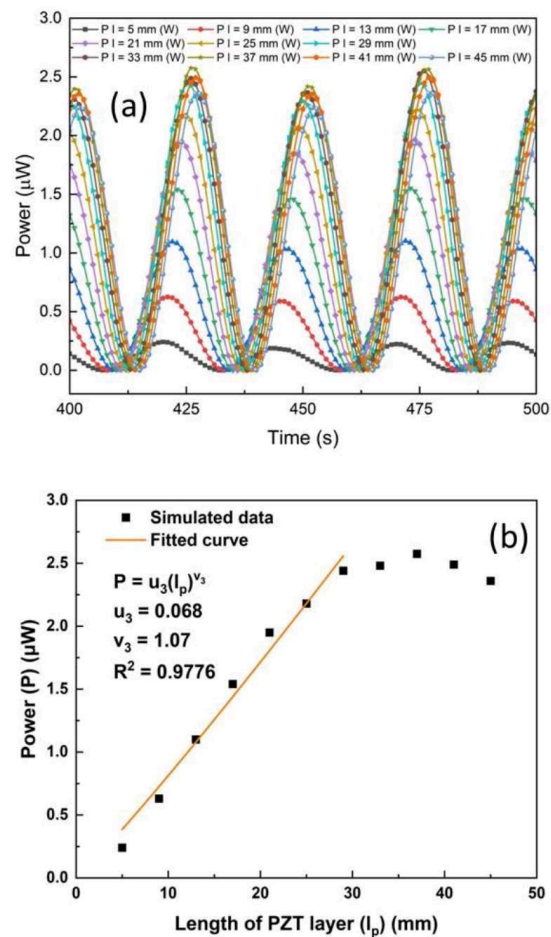


Figure 4.6 (a) represents the variation or power with time by changing the length of PZT, and (b) the Effect of PZT length on power generated in bimetallic piezoelectric energy harvester.

From Figure 4.6 (a) and Figure 4.6 (b), it is observed that as the length of PZT increases, the power is also increased. It is because as length increases, the surface area of PZT increases and from equation 2.15. It is found that power is directly proportional to the surface area of PZT. Hence power increases with the length of PZT increase [20].

4.4 Power variation with a position of PZT patch

The length of the PZT patch is fixed at 29 mm and now varies the position of the PZT patch from the fixed end to the last end. We measured the distance of the patch from the fixed end, which is assigned as $x = 0$, and to the last end $x = 21$ mm. Patch shifts from fixed end to free end with a distance of 3 mm.

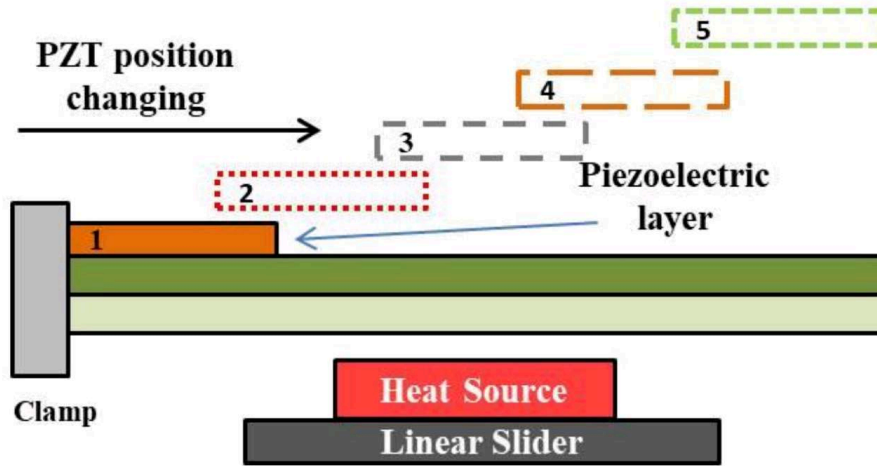


Figure 4.7: Schematic diagram shows piezoelectric patch position changing.

Figure 4.8 (a) shows the variation of power with time at different positions of PZT. Figure 4.8 (b) represents the data obtained from the simulation. A curve fits all the data, correlating the power variations and the piezoelectric patch's distance from the fixed end. As the distance of the piezoelectric patch increases from the fixed end, the power initially increases and achieves the peak value at $x = 18$ mm, then power decreases. It is due the fact that the generation of stress on the piezoelectric layer is due to two reasons (a) The maximum stress generated at the fixed end of the cantilever beam and (b) The stress

generated due to the deflection of the bimetallic beam at the center position. Hence in the present analysis, the position of the piezoelectric layer was a combined effect of these two reasons.

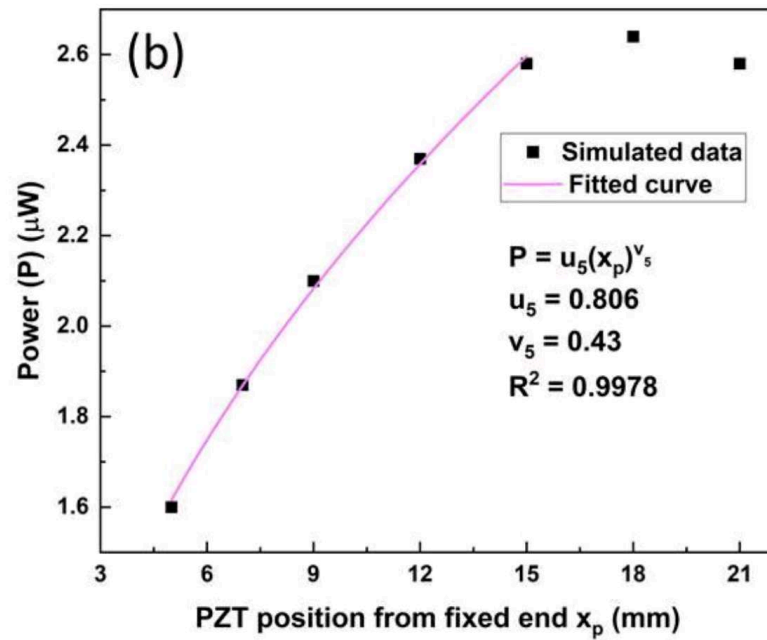
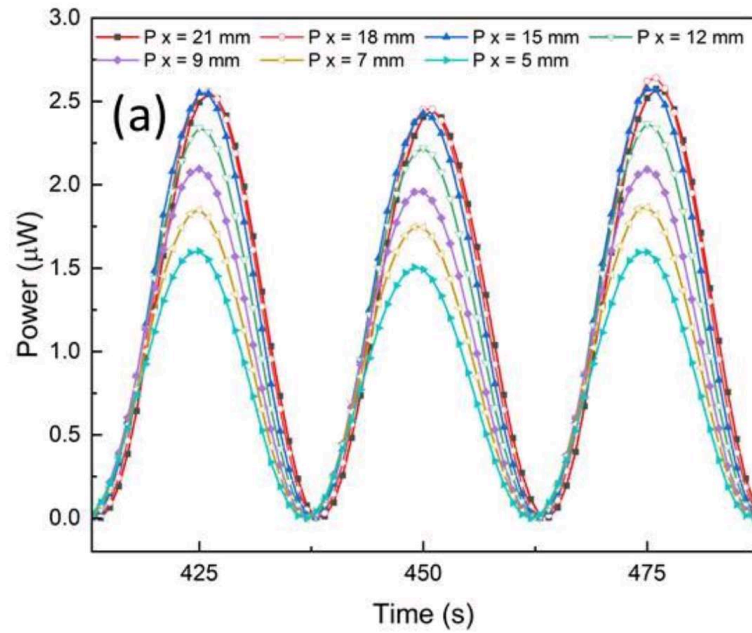


Figure 4.8 (a): Power as a function of time at different positions of PZT and (b) effect of PZT position on power generated in bimetallic piezoelectric energy harvester.

4.5 Power variation with the width of PZT and Beam

The length of the PZT patch is fixed at 29 mm and is kept at the central portion of the bimetallic beam. The length of the heat source is 40 mm and placed along the width of the bimetallic-based piezoelectric energy harvester. The variation of power with the width of the PZT patch is observed in this simulation. Since the piezoelectric patch is placed over the beam, the width of the beam and PZT increase by an equal amount. The width of the patch and beam is increased from 5 mm to 50 mm up beyond the length of the beam. The schematic of PZT and beam width increases is shown in Figure 4.9.

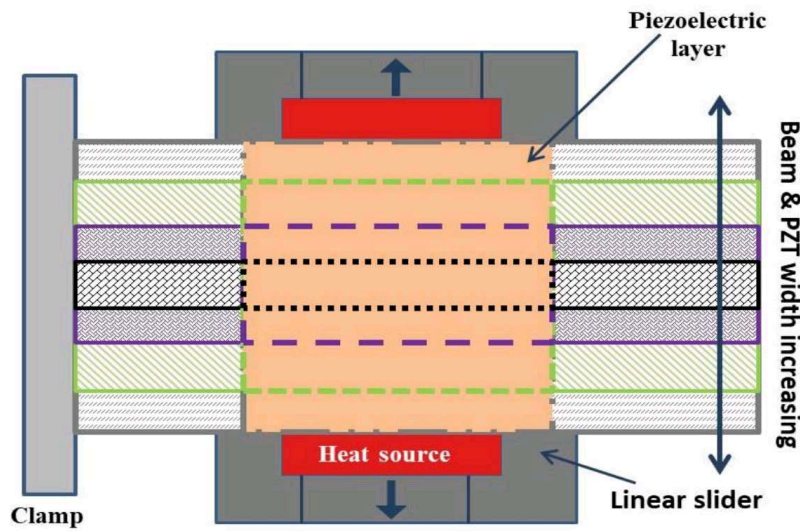


Figure 4.9: Schematic of increase in width of piezoelectric patch and beam.

Figure 4.10 (a) shows the power variation with time at different PZT and beam widths. Figure 4.10 (b) shows the effect of the width of the beam and PZT on power generated in a bimetallic-based piezoelectric energy harvester. It also shows the relation between the power and width of PZT. It is observed that as the width of PZT and beam increases up to the length of the heat source i.e., 40 mm, the power increases and beyond the length of the heat source, the power decreases. It is because the contact area of the bimetallic beam increases with the beam and when the width of the beam is equal to the

length of the heat source, maximum power is obtained beyond that power decreases.

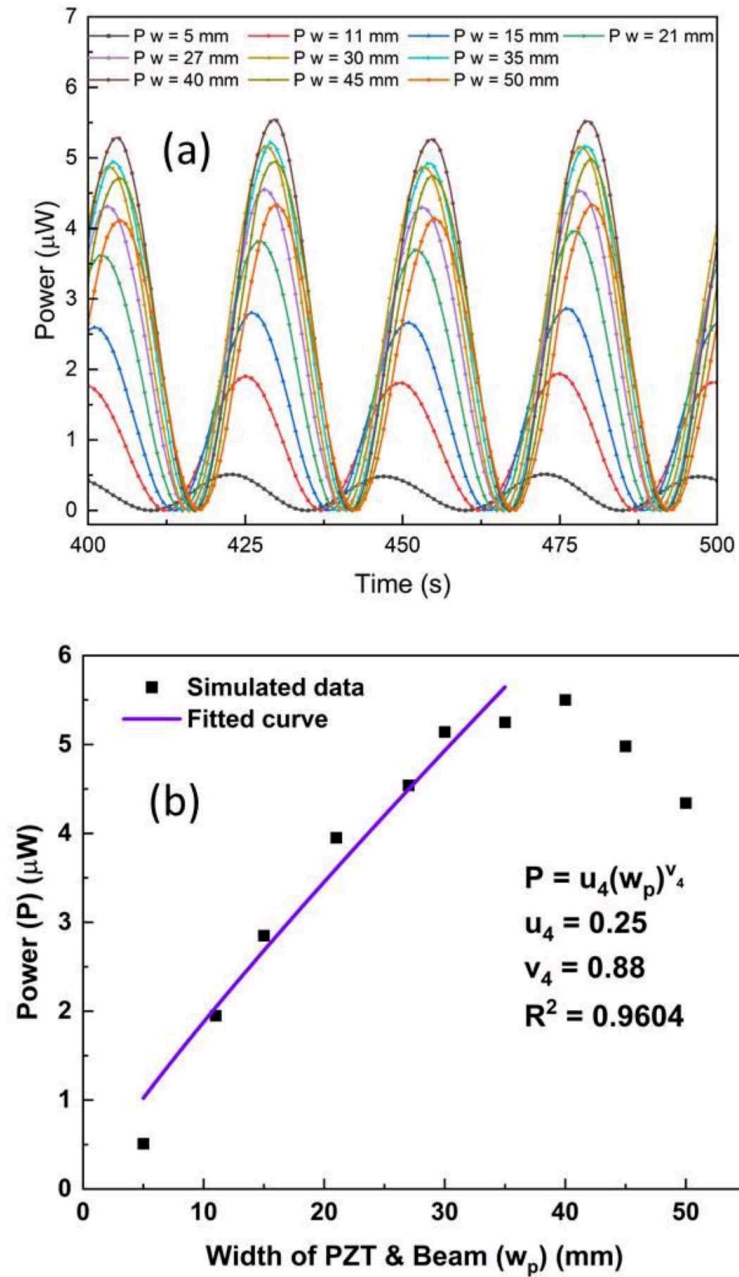


Figure 4.10 (a): Plots of power as a function of time at various widths of PZT and beam, (b) effect of PZT and beam width on power generated in bimetallic piezoelectric energy harvester.

Chapter 5: Conclusion and future scope

The simulation is done at the optimum resistance of 100 M Ω . All the variation is done, and results are observed at each parameter in the geometry of the bimetallic-based piezoelectric energy harvester and at the properties of bimetal used in the energy harvester.

- ❖ Variation with substrate material (bimetal) properties.
 - As the source temperature increases, the beam temperature also increases linearly. Power also increases with beam temperature.
 - As the difference in the CTE of both layers of bimetal increases, the power also increases.
 - By keeping the thermal conductivity of the upper layer at a fixed value and changing the thermal conductivity of the lower layer in increasing order, the difference in the thermal conductivity increases. As the difference in thermal conductivity increases, the power decreases.
 - By keeping the density of the upper layer at a fixed value and changing the density of the lower layer in increasing order, the difference in the density increases. As the difference in density increases, the power decreases.
- ❖ Power variation with the geometric parameter of energy harvester
 - As the thickness of the bimetal beam increases, power and stress decrease.
 - As the thickness of PZT increases, power decreases.
 - As the length of PZT increases the power increases.
 - As the distance of PZT from fixed is increases, the power initially increases then decreases.
 - As the width of the beam and PZT increases, the power initially increases until the length of the heat source, then beyond the length of the heat source, power decreases.

The relation from both the variation is obtained, shown below.

5.1 Conclusions

Substrate material parameter variation relation is found as

$$P = C_1(\Delta\alpha)^{3.37}(\Delta k)^{-0.31}(\Delta\rho)^{-0.75}(\Delta T)^{1.95}$$

Where $C_1 = 1.37 \times 10^{-7}$. Check our relation with simulated results keeping $\Delta k = 40$; $\Delta\rho = 5000$; $\Delta T = 9$ K constant and vary $\Delta\alpha$ from 20 to 8. We are obtaining the same trend as obtained in the simulation.

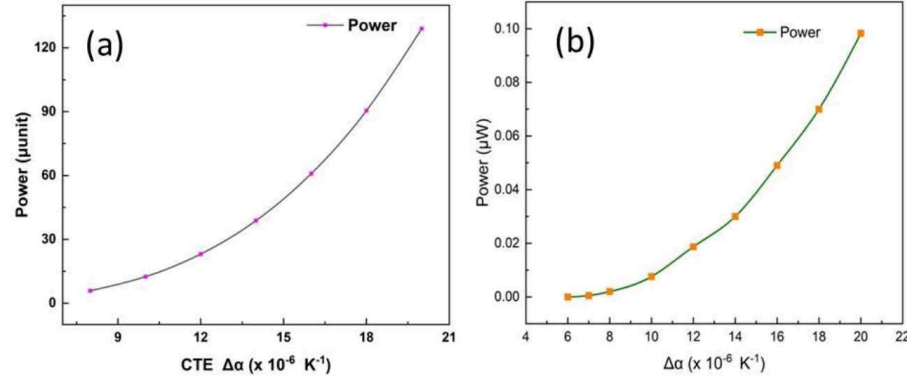


Figure 5.1: Variation of power with CTE (a) obtained from the relation and (b) obtained from the simulation

Geometric Parameter Variation for power is found as

$$P = C_2(x_p)^{0.43}(l_p)^{1.07}(t_s)^{-1.3}(t_p)^{-1.12}(w_p)^{0.88}$$

Where $C_2 = 1.788 \times 10^{-5}$. In order to check our relation with simulated results keeping $x_p = 15$; $l_p = 29$; $t_s = 0.2$, $w_p = 20$ constant and vary PZT thickness from 0.1 to 0.7

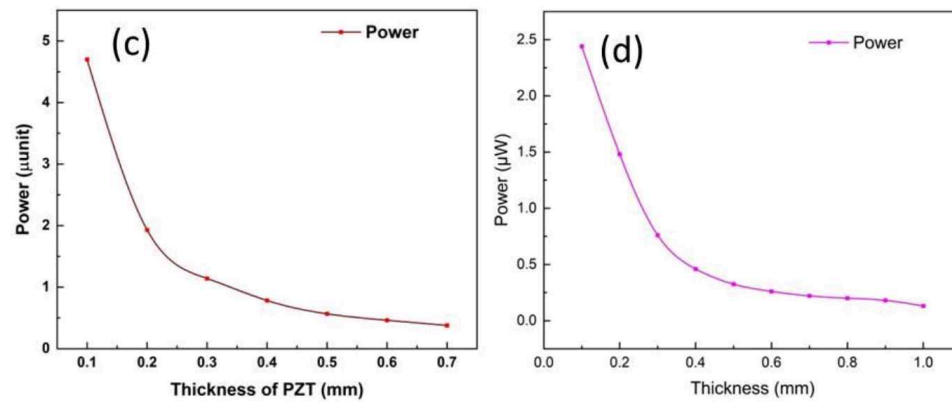


Figure 5.1: Power variation with a PZT (c) thickness obtained from the relation and (d) obtained from the simulation.

5.2 Future scope:

- Mathematical modeling is required for converting the obtained power relation into dimensionless terms to quickly determine the exact value for the particular conditions of the bimetallic thermal energy harvester.
- Experimental validation is required for the obtained empirical power relations.

References

1. Bowen, C., et al., Piezoelectric and ferroelectric materials and structures for energy harvesting applications. *Energy and Environmental Science*, 2014. 7(1): p. 25-44.
2. Katzir, S., The discovery of the piezoelectric effect. *The Beginnings of Piezoelectricity: A Study in Mundane Physics*, 2006: p. 15-64.
3. Bera, B. and M.D. Sarkar, Piezoelectric effect, piezotronics and piezophotonics: a review. *Imperial Journal of Interdisciplinary Research (IJIR)*, 2016. 2(11): p. 1407-1410.
4. Bassett, C.A.L., Biologic significance of piezoelectricity. *Calcified tissue research*, 1967. 1(1): p. 252-272.
5. Chauhan, A., R. Vaish, and C. Bowen, Piezoelectric material selection for ultrasonic transducer and actuator applications. *Proceedings of the Institution of Mechanical Engineers, Part L: Journal of Materials: Design and Applications*, 2015. 229(1): p. 3-12.
6. Asan, A.S., An electromechanical system for characterization of piezoelectric materials. 2016.
7. De Jong, M., et al., A database to enable discovery and design of piezoelectric materials. *Scientific data*, 2015. 2(1): p. 1-13.
8. Wang, Y., et al., Enhanced Piezoelectric Properties Enabled by Engineered Low-Dimensional Nanomaterials. *ACS Applied Nano Materials*, 2022. 5(9): p. 12126-12142.
9. Safaei, M., H.A. Sodano, and S.R. Anton, A review of energy harvesting using piezoelectric materials: state-of-the-art a decade later (2008–2018). *Smart materials and structures*, 2019. 28(11): p. 113001.
10. Dineva, P., et al., *Piezoelectric materials*. 2014: Springer.
11. Bora, P.N., *Cavitation studies of lumbar zygapophysial joints using vibration measurements*. 2011: Auburn University.

12. Bohm, J., et al., Czochralski growth and characterization of piezoelectric single crystals with langasite structure: $\text{La}_3\text{Ga}_5\text{SiO}_{14}$ (LGS), $\text{La}_3\text{Ga}_5.5\text{Nb}_{0.5}\text{O}_{14}$ (LGN) and $\text{La}_3\text{Ga}_5.5\text{Ta}_{0.5}\text{O}_{14}$ (LGT) II. Piezoelectric and elastic properties. *Journal of crystal growth*, 2000. 216(1-4): p. 293-298.
13. Polla, D.L. and L.F. Francis, Processing and characterization of piezoelectric materials and integration into microelectromechanical systems. *Annual review of materials science*, 1998. 28(1): p. 563-597.
14. Linnemann, K., S. Klinkel, and W. Wagner, A constitutive model for magnetostrictive and piezoelectric materials. *International Journal of Solids and Structures*, 2009. 46(5): p. 1149-1166.
15. Li, H., C. Tian, and Z.D. Deng, Energy harvesting from low frequency applications using piezoelectric materials. *Applied physics reviews*, 2014. 1(4): p. 041301.
16. Kim, H.S., J.-H. Kim, and J. Kim, A review of piezoelectric energy harvesting based on vibration. *International journal of precision engineering and manufacturing*, 2011. 12: p. 1129-1141.
17. Covaci, C. and A. Gontean, Piezoelectric energy harvesting solutions: A review. *Sensors*, 2020. 20(12): p. 3512.
18. Calìò, R., et al., Piezoelectric energy harvesting solutions. *Sensors*, 2014. 14(3): p. 4755-4790.
19. Priya, S., et al., A review on piezoelectric energy harvesting: materials, methods, and circuits. *Energy Harvesting and Systems*, 2017. 4(1): p. 3-39.
20. Lee, F.Y., A. Navid, and L. Pilon, Pyroelectric waste heat energy harvesting using heat conduction. *Applied thermal engineering*, 2012. 37: p. 30-37.
21. Nozariasbmarz, A., et al., Review of wearable thermoelectric energy harvesting: From body temperature to electronic systems. *Applied Energy*, 2020. 258: p. 114069.

22. He, W., et al., Recent development and application of thermoelectric generator and cooler. *Applied Energy*, 2015. 143: p. 1-25.
23. Bell, L.E., Cooling, heating, generating power, and recovering waste heat with thermoelectric systems. *Science*, 2008. 321(5895): p. 1457-1461.
24. Xie, J., et al., Performance of thin piezoelectric materials for pyroelectric energy harvesting. *Journal of Intelligent Material Systems and Structures*, 2010. 21(3): p. 243-249.
25. Bowen, C.R., et al., Pyroelectric materials and devices for energy harvesting applications. *Energy and Environmental Science*, 2014. 7(12): p. 3836-3856.
26. McKinley, I.M., F.Y. Lee, and L. Pilon, A novel thermomechanical energy conversion cycle. *Applied energy*, 2014. 126: p. 78-89.
27. Hunter, S.R., et al. Development of MEMS based pyroelectric thermal energy harvesters. in *Energy Harvesting and Storage: Materials, Devices, and Applications II*. 2011. SPIE.
28. Ravindran, S., et al., A self-sustaining micro thermomechanic-pyroelectric generator. *Applied Physics Letters*, 2011. 99(10): p. 104102.
29. Cottrill, A.L., et al., Persistent energy harvesting in the harsh desert environment using a thermal resonance device: Design, testing, and analysis. *Applied Energy*, 2019. 235: p. 1514-1523.
30. Chun, J., et al., Thermo-magneto-electric generator arrays for active heat recovery system. *Scientific reports*, 2017. 7(1): p. 41383.
31. Zhang, Z., et al., Management and storage of energy converted via a pyroelectric heat engine. *Applied Energy*, 2018. 230: p. 1326-1331.
32. Gusarov, B., et al., Thermal energy harvesting by piezoelectric PVDF polymer coupled with shape memory alloy. *Sensors and Actuators A: Physical*, 2016. 243: p. 175-181.

33. Lee, J.H., et al., Highly stretchable piezoelectric-pyroelectric hybrid nanogenerator. *Advanced Materials*, 2014. 26(5): p. 765-769.
34. You, M.-H., et al., A self-powered flexible hybrid piezoelectric–pyroelectric nanogenerator based on non-woven nanofiber membranes. *Journal of Materials Chemistry A*, 2018. 6(8): p. 3500-3509.
35. Kim, M.-S., et al., Design of wearable hybrid generator for harvesting heat energy from human body depending on physiological activity. *Smart Materials and Structures*, 2017. 26(9): p. 095046.
36. Kang, M. and E.M. Yeatman, Coupling of piezo-and pyroelectric effects in miniature thermal energy harvesters. *Applied Energy*, 2020. 262: p. 114496.